

# Paleoceanography and Paleoclimatology

## RESEARCH ARTICLE

10.1029/2020PA004145

### Key Points:

- Bermudan climate during the Last Interglacial period (MIS 5e) was colder than today
- Subannual clumped isotope analyses capture seasonal-scale changes in temperature and water composition
- Variable discharge from an underground aquifer affects oxygen isotopic composition of coastal water during MIS 5e and today

### Supporting Information:

Supporting Information may be found in the online version of this article.

### Correspondence to:

J. Z. Zhang,  
jadezz@umich.edu





### Citation:

Zhang, J. Z., Petersen, S. V., Winkelstern, I. Z., & Lohmann, K. C. (2021). Seasonally variable aquifer discharge and cooler climate in Bermuda during the last interglacial revealed by subannual clumped isotope analysis. *Paleoceanography and Paleoclimatology*, 36, e2020PA004145. <https://doi.org/10.1029/2020PA004145>

Received 16 OCT 2020

Accepted 5 MAY 2021

## Seasonally Variable Aquifer Discharge and Cooler Climate in Bermuda During the Last Interglacial Revealed by Subannual Clumped Isotope Analysis

Jade Z. Zhang<sup>1</sup> , Sierra V. Petersen<sup>1</sup> , Ian Z. Winkelstern<sup>2</sup> , and Kyger C. Lohmann<sup>1</sup> 

<sup>1</sup>Department of Earth and Environmental Science, University of Michigan, Ann Arbor, MI, USA, <sup>2</sup>Department of Geology, Grand Valley State University, Allendale, MI, USA

**Abstract** Faunal analog reconstructions suggest that Last Interglacial (MIS 5e) sea surface temperatures were cooler around Bermuda and in the Caribbean than modern climate. Here we describe new and revised clumped isotope measurements of *Cittarium pica* fossil shells supporting previous findings of cooler than modern temperatures in Bermuda during the Last Interglacial. We resolve temperature and  $\delta^{18}\text{O}_w$  differences between two closely located and apparently coeval sites described in Winkelstern et al. (2017), <https://doi.org/10.1002/2016pa003014> through reprocessing raw isotopic data with the updated Brand/IUPAC parameters. New subannual-resolution clumped isotope data reveal large variations in  $\delta^{18}\text{O}_w$  out of phase with seasonal temperature changes (i.e., lower  $\delta^{18}\text{O}_w$  values in winter). Supported by modern  $\delta^{18}\text{O}_w$  measurements identifying similar processes occurring today, we suggest past variations in coastal  $\delta^{18}\text{O}_w$  were driven by seasonally variable freshwater discharge from a subterranean aquifer beneath the island. Taken together, our results emphasize the importance of  $\delta^{18}\text{O}_w$  in controlling carbonate  $\delta^{18}\text{O}$ , and suggest that typical assumptions of constant  $\delta^{18}\text{O}_w$  should be made cautiously in nearshore settings and can contribute to less accurate reconstructions of paleotemperature.

## 1. Introduction

The Last Interglacial (Marine Isotope Stage 5e, or MIS 5e) is the most recent time in which global mean surface temperatures exceeded modern values, reaching  $\sim 2^\circ\text{C}$  warmer than present (CLIMAP, 1984; Kaspar et al., 2005; Kukla et al., 2002; Turney & Jones, 2010; Sanchez Goni et al., 2012). Reconstructions of MIS 5e sea surface temperature (SST) as part of the CLIMAP project and subsequent studies found that the oceans were not uniformly warmer during this time (Brocas et al., 2019; CLIMAP, 1984; Harrison et al., 1994; Turney & Jones, 2010). Instead, regional-scale spatial patterns were revealed showing a generally cooler reconstructed Central Atlantic and Caribbean temperatures (with the exception of one study showing warmer than Holocene in the Caribbean; Schmidt et al., 2004) and warmer reconstructed conditions in the North Atlantic and Greenland/Iceland/Nordic Sea (Brocas et al., 2019; CLIMAP, 1984; Turney & Jones, 2010), suggesting differences in meridional heat transport relative to today. The island of Bermuda ( $32.4^\circ\text{N}$ ,  $64.8^\circ\text{W}$ ) sits near this paleo-interface, with cooler-than-modern regions to the south and warmer-than-modern regions to the north.

Today, as a result of the warm Gulf Stream Current that contours along the U.S. East Coast, Bermuda has a warm subtropical climate that defies its latitude and makes it the northern-most Atlantic location where coral reefs grow (Coates et al., 2013). The annual average SST is  $23^\circ\text{C}$  and the throughout the year temperature ranges from  $19^\circ\text{C}$ – $29^\circ\text{C}$  (lowest monthly mean to highest monthly mean - NOAA National Data Buoy Center), compared to  $4^\circ\text{C}$ – $28^\circ\text{C}$  in coastal Charleston, South Carolina at the same latitude (US Climate Data 2019) (<https://www.usclimatedata.com/>).

Sediments on Bermuda consist of layered eolianites, marine limestones and terra rosa paleosols (Coates et al., 2013). During warm, interglacial periods, carbonates formed across an expanded platform submerged by higher sea level; during glacial periods, eolianites formed as coastal dunes covered a larger island area exposed by lower sea level (Meischner et al., 1995). Today, marine carbonates exposed  $\sim 0$ – $5$  m above the modern water line contain fossil shells and corals that can be dated and used for paleoclimate reconstructions. The stratigraphy of Bermuda has been well characterized, considered and refined over the years (Hearty, 2002; Hearty & Olson, 2010; Hearty et al., 2004; Land et al., 1967; Muhs et al., 2002; Rowe

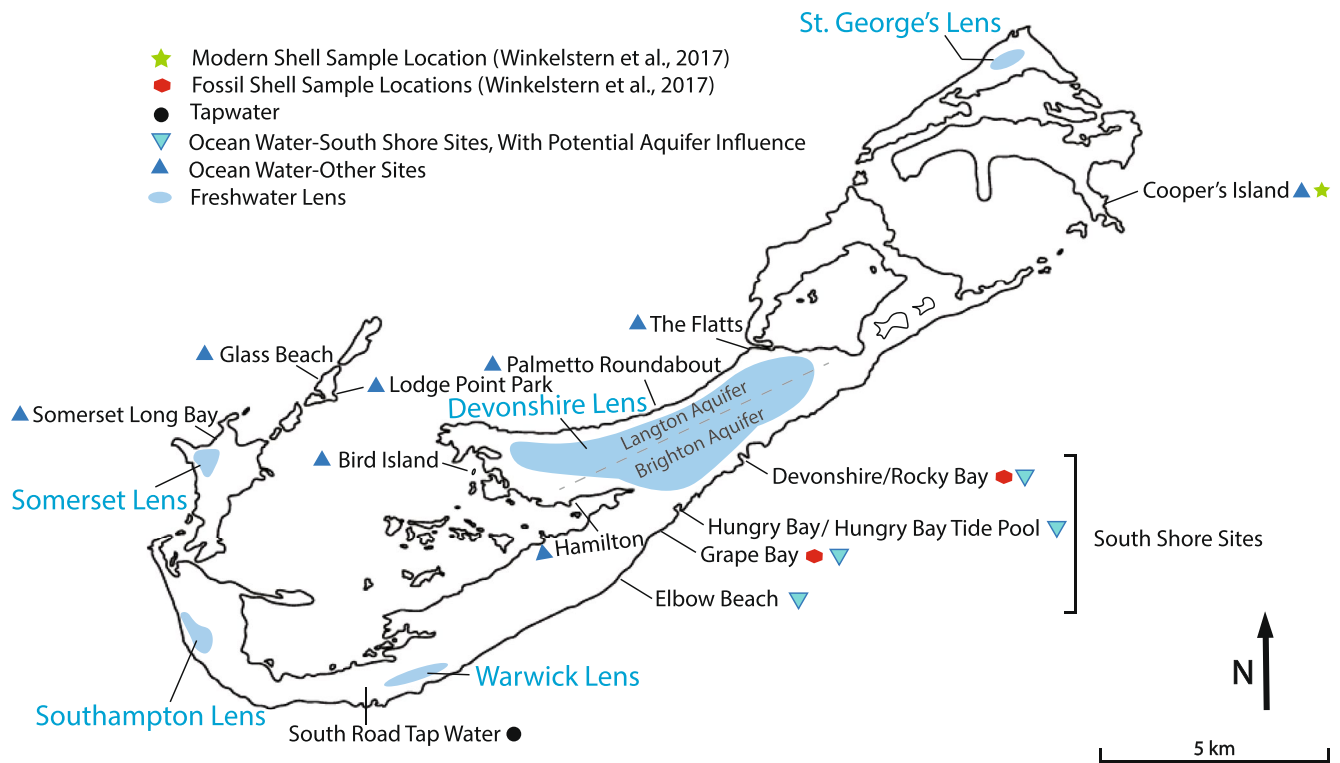


**Figure 1.** Map of Bermuda showing the location of freshwater aquifers, seawater, tap water and lake/pond waters collected across the island. Fossil and modern shell collection sites also shown for comparison. Freshwater lens locations are from Vacher (1978) and van Hengstum and Scott (2012).

et al., 2014). Geochronological techniques including Amino Acid Racemization, Uranium-Thorium dating, and seismic imaging (Harmon et al., 1983; Hearty et al., 1992, 1999; Rowe et al., 2014; Vollbrecht, 1990) have led to a robust age model assigning marine deposits to the last several interglacial intervals. Limestone units on the island can now be divided into five main Formations, in ascending order: Walsingham (>700,000 ka, >MIS 13), Town Hill (~400,000 ka, MIS 11), Belmont (~200,000 ka, MIS 7), Rocky Bay (~120,000 ka, MIS 5e) and Southampton Formations (~80,000 ka, MIS 5a). In particular, the Devonshire Marine Member of the Rocky Bay Formation has been dated to the MIS 5e, based on numerous stratigraphic and dating efforts using multiple techniques mentioned above (Hearty, 2002; Hearty and Olson, 2010; Hearty et al., 2004; Land et al., 1967; Muhs et al., 2002; Rowe et al., 2014).

*Cittarium pica* (*C. pica*), also known as the West Indian top-shell, is a distinct, fast-growing, intertidal gastropod that inhabits crevices and small protected areas of exposed rocky shores (Olson & Hearty, 2013; Robertson, 2003). This species occurs today in Bermuda, throughout the Caribbean and in Central America. In Bermuda, abundant, well preserved *C. pica* fossils can be found in the marine limestones deposited along past rocky shores during multiple prior interglacial stages, specifically MIS 11, 9, 5e and 1 (Olson & Hearty, 2013; Walker, 1994). All fossil *C. pica* mentioned in this study were collected from the Devonshire Marine Member of the Rocky Bay Formation (MIS 5e).

Due to the small size of the island, there are no freshwater lakes or rivers, but freshwater collects in subsurface lenses that discharge directly into the surrounding oceans below the waterline (Rowe, 1984; Vacher, 1978; Figure 1). Bermuda has multiple subsurface freshwater lenses, the largest one being the Devonshire Lens or Central Lens under Devonshire, Smith's and Paget parishes. This lens covers an area more than twice that of the other freshwater lenses combined (Rowe, 1984). Large differences in permeability in the hydrostratigraphic units containing the aquifer (hydraulic conductivity of 30–120 m/day in the Langton Aquifer on the north side of the island vs. 1,000 m/day in the Brighton Aquifer on the south side of the island) leads to an asymmetrically shaped lens in cross section and impedes the escape of freshwater to the oceans on the north shore versus the south shore (Vacher & Rowe, 1997).

A previous paleoclimate study reconstructed cooler-than-modern SSTs during MIS 5e at two sites in Bermuda using subannual stable isotopes and bulk clumped isotopes on gastropod fossils of the species *C. pica* (Winkelstern et al., 2017). Reconstructed paleotemperatures differed significantly between the two sites, despite their close proximity (~2 km apart) and apparently equivalent geologic age (based on stratigraphic correlation and limited radiometric age dating). Samples from Grape Bay (GB) recorded significantly cooler temperatures (~10°C cooler than today) compared to samples from Devonshire Bay/Rocky Bay (DB/RB) (~5°C cooler than today). Both the large apparent temperature difference between the two sites and the extreme level of cooling relative to today were difficult to explain. The authors proposed that cool, fresh, isotopically depleted waters from the melting Greenland Ice Sheet could have traveled southward and temporarily cooled and lowered the isotopic composition of coastal waters around Bermuda (Winkelstern et al., 2017).

Here, we present new, subannual-scale clumped isotope measurements on five of the ten *C. pica* shells from the original study (1 modern, 2 fossils from DB/RB, 2 fossils from GB) to investigate the seasonal persistence and timing of interglacial cooling and determine whether inter-site differences may have been the result of seasonal sampling bias. Published clumped isotope data from Winkelstern et al. (2017) were recalculated using improved data processing techniques (IUPAC/Brand parameters; see Petersen et al., 2019) for more accuracy and to enable better comparison with new data. Finally, we present  $\delta^{18}\text{O}$  of modern waters (tap and marine) from 16 locations around the island and compare with reconstructed  $\delta^{18}\text{O}_w$  based on clumped isotope measurements. Our findings, combining new subannual clumped isotope measurements reprocessed published data, and these modern water data, point to the importance of seasonal variations in  $\delta^{18}\text{O}_w$  over temperature in controlling carbonate  $\delta^{18}\text{O}$ . They also highlight that typical assumptions of seasonally invariant  $\delta^{18}\text{O}_w$  should be made cautiously, even in settings like Bermuda that have nearly zero above-ground (riverine) freshwater runoff.

## 2. Materials and Methods

### 2.1. Sample Selection and Sampling Strategy

Carbonate clumped isotope paleothermometry ( $\Delta_{47}$ ) is a thermodynamically based proxy founded on the temperature dependence of the abundance of  $^{13}\text{C}$ - $^{18}\text{O}$  bonds in the carbonate mineral lattice (Eiler, 2007, 2011). At colder temperatures, these rare and heavy isotopes clump together at a level higher than expected by the stochastic (random) distribution of these isotopes, denoted as  $\Delta_{47}$  based on the occurrence of mass-47  $\text{CO}_2$  (containing both heavy isotopes) produced from acid-digestion of carbonate (Affek, 2012; Huntington et al., 2009). While traditional  $\delta^{18}\text{O}$ -based thermometry requires knowledge of the  $\delta^{18}\text{O}$  of the precipitating fluid ( $\delta^{18}\text{O}_w$ ) to accurately reconstruct past climate, the clumped isotope method has the ability to reconstruct a sample's formation temperature,  $\delta^{18}\text{O}$ ,  $\delta^{13}\text{C}$ , and  $\delta^{18}\text{O}_w$  with a single measurement (Eiler, 2011; Ghosh et al., 2006). In mollusk shells like the gastropod *C. pica*, clumped isotopic sampling along the direction of growth can reveal subannual changes in carbonate  $\delta^{18}\text{O}$ , temperature and  $\delta^{18}\text{O}_w$  (via  $\Delta_{47}$ ).

Mollusk shells act as high-resolution archives of paleoenvironmental information and the geochemistry of mollusk shells has often been used to reconstruct paleotemperature (Grossman & Ku, 1986; A. Tripathi et al., 2001; Wanamaker et al., 2006; Eagle et al., 2013). However, in certain cases, carbonate-secreting organisms (e.g., corals, brachiopods) do not precipitate their skeletons in equilibrium with the ambient environment, leading to inaccurate estimations of paleoenvironmental conditions (Bajnai et al., 2018; Eagle et al., 2010; Thiagarajan et al., 2011; A. K. Tripathi et al., 2010; Saenger et al., 2012). To date, isotopic vital effects have not been identified in any mollusk species (Eagle et al., 2013; Henkes et al., 2013; Winkelstern et al., 2017).

A total of six well-preserved *C. pica* shells collected, described, and analyzed by Winkelstern et al. (2017) were resampled for this study: two modern specimens from Cooper's Island, two MIS 5e fossil shells each from Devonshire/Rocky Bay and GB (Figure 1). A third modern specimen (BM3), collected alongside the other two modern shells as part of the original study but never analyzed, was added to make a total of seven shells studied. As part of the original study, the first six shells were micro-sampled at high resolution for  $\delta^{18}\text{O}$  and bulk sampled for clumped isotope ( $\Delta_{47}$ ) analysis at a single point near the aperture. These original  $\Delta_{47}$  analyses therefore reflected the last shell growth for each organism.

In our current study, additional high resolution  $\delta^{18}\text{O}$  sampling was conducted on two previously sampled modern shells (BM1, BM2) to extend the published high-resolution record by 1–2 more years. The third modern shell (BM3) was sliced along the last growth whorl to reveal a cross section of growth using a rock saw, and four years of growth were sampled for high-resolution  $\delta^{18}\text{O}$ . Three or more new clumped isotope measurements were made per fossil shell, targeting the highest and lowest  $\delta^{18}\text{O}_{\text{carb}}$  values, as recorded in published (Winkelstern et al., 2017) and newly expanded high resolution  $\delta^{18}\text{O}$  records, with the goal of capturing the full seasonal range in temperature and the oxygen isotopic composition of water ( $\delta^{18}\text{O}_{\text{w}}$ ) while further ensuring *C. pica* could accurately record seasonality and serve as a climate proxy for the past. Ten additional  $\Delta_{47}$  measurements were made on the modern shell BM2.

Winkelstern et al. (2017) used multiple methods to determine these fossil shells were well preserved. As part of the original study, fossil shells were inspected under the microscope, powders were analyzed with X-ray diffraction, and isotopic analyses of fossils were compared to surrounding bulk material. All fossil samples exhibited excellent preservation, displaying original shell layering and coloration, preserving a 100% aragonitic composition, and retaining contrasting  $\delta^{18}\text{O}$  and clumped isotope values relative to co-occurring diagenetic cements (Winkelstern et al., 2017). All isotopic samples were taken from the pristine inner shell material from cross section (Figure S1) to avoid the outermost layer that could have been physically abraded, encrusted, or bored by predators. Burial history of these units is negligible – MIS 5e rocks are stranded ~0–5m above modern sea level in their original position and have never been buried or heated, eliminating the possibility of clumped isotopic bond reordering (Henkes et al., 2014; Stolper & Eiler., 2015). All tests mentioned above point to the unlikelihood of diagenetic alteration of the studied fossil shells, and thus no further tests on diagenesis were deemed necessary for the purpose of this study. Previous work on Bermudan fossil corals also supports excellent preservation and closed-system behavior (e.g., Muhs et al., 2002).

## 2.2. High Resolution Stable Isotope Analytical Methods

High-resolution drilling was carried out with a Merchantek MicroMill computer-controlled drilling stage to collect ~50  $\mu\text{g}$  of powder for each analysis (Figure S1), spaced every ~3 mm, resulting in ~20 points per year of growth. Each powder was analyzed for  $\delta^{13}\text{C}$  and  $\delta^{18}\text{O}$  using a Kiel IV automated carbonate device attached to a Thermo-Finnegan MAT 253 dual inlet mass spectrometer. Data was standardized by comparison to NBS-18 and NBS-19 with units reported in per mille (‰), relative to the VPDB standard, with a typical uncertainty of  $\pm 0.1\text{‰}$  in both  $\delta^{13}\text{C}$  and  $\delta^{18}\text{O}$ .

## 2.3. Clumped Isotope Analytical Methods

Seasonal peak and trough points were identified in the high resolution  $\delta^{18}\text{O}$  data for each shell. Each identified  $\delta^{18}\text{O}$  maximum or minimum was sampled using a low speed dental drill until a total of 20 mg was collected and homogenized (Figure S1). Individual sample replicates of 4–6 mg were reacted in phosphoric acid to produce  $\text{CO}_2$  and purified using a custom-built vacuum line described by Defliese et al. (2015) with procedures further described in Petersen et al. (2016). More details of the procedure can be found in the supplement (Text S2). All samples were replicated three or more times, with most samples replicated four times, spread out over a period of months to accommodate long-term variation in mass spectrometer behavior.

$\Delta_{47}$  was calculated from raw voltages using an R-code script applying the updated Brand parameters (Petersen et al., 2019).  $\Delta_{47}$  values were converted into the absolute reference frame to correct the dependency of the measured  $\Delta_{47}$  on  $\delta_{47}$  and mass spectrometer “frame compression/stretching” using heated (1000°C) and equilibrated (25°C) gas standards (Dennis et al., 2011). An acid fractionation factor of +0.072‰ corresponding to a reaction temperature of 75°C was applied to account for the isotopic fractionation resulting from loss of one oxygen atom during acid digestion (Petersen et al., 2019). Three in-house carbonate standards (Carrara marble and aragonitic ooids (Defliese et al., 2015), and an aragonitic coral standard CORS (Rosenheim et al., 2013) were monitored and correction windows were adjusted to minimize drift in corrected standard values through time. True values for these standards were separately defined relative to the ETH standards. A secondary transfer function using many replicates of these three standards, plus a handful of

replicates of ETH1-4, was applied to bring final  $\Delta_{47}$  values into alignment with the current best community-wide reference frame (see Text S2).

Individual replicates were determined to be bad if  $\Delta_{48}$  values were elevated more than 2‰ above pure gas standards indicating contamination. Within each sample, if the standard deviation of all replicates was in excess of the long-term standard deviation of in-house carbonate standards (0.025‰), the most deviant replicate was deemed an outlier and removed, which in most cases corresponded to a single-replicate temperature of  $>50^{\circ}\text{C}$  or  $<-15^{\circ}\text{C}$ , likely resulting from individual errors during sample preparation. After this screening, only samples with at least three good replicates were included for interpretation.

$\Delta_{47}$  values were converted to temperature using the synthetic composite calibration of Petersen et al. (2019) with Brand/IUPAC parameters, updated  $\Delta_{47\text{-TE}}$  values and acid digestion fractionation values ( $\Delta_{47\text{-RFAC(Br,P,newAFF)}} = (0.0383 \pm 1.7 \text{ E}^{-6}) * (10^6/\text{T}^2) + (0.258 \pm 1.7 \text{ E}^{-5})$ ). This calibration equation was chosen because it reflects the growing calibration consensus in the clumped isotope community and our modern shell samples presented here produced best results using this calibration.

$\delta^{18}\text{O}_{\text{carb}}$  values were combined with  $\Delta_{47}$ -temperatures to calculate  $\delta^{18}\text{O}_{\text{w}}$  using both the mollusk-specific aragonite-water fractionation factor of Grossman and Ku (1986) and the water-aragonite fractionation factor of Kim et al. (2007) based on synthetic laboratory precipitates. The first equation was chosen because the relationship is defined based on aragonitic mollusks, including gastropods, matching our specimen type (Grossman & Ku, 1986). The second equation of Kim et al. (2007) is a targeted laboratory study on the temperature dependence of mineral-specific acid fractionation factors and is commonly used for many aragonitic taxa. Both equations were explored for our data set but we chose to present our data in this study with Grossman and Ku (1986) because this produced the best alignment between our modern shells and modern instrumental temperatures (see Discussion).  $\delta^{18}\text{O}_{\text{w}}$  values calculated using Kim et al. (2007) can be found in the supplementary material.

#### 2.4. Reprocessing of Published Clumped Isotope Data

Original  $\Delta_{47}$  values and temperatures calculated by Winkelstern et al. (2017) were processed using Santrock/Gonfiantini parameters following Huntington et al. (2009),  $\Delta_{47\text{-TE}}$  values from Dennis et al., (2011), and the acid fractionation factor and temperature calibration of Defliese et al., (2015). Since the time of publication, many of these values have been updated (Petersen et al., 2019). Therefore, we reprocessed the Winkelstern et al. (2017) data from raw voltages using the same R-code as new data, this time employing Brand/IUPAC parameters, updated  $\Delta_{47\text{-TE}}$  values and acid fractionation factor from Petersen et al. (2019). It was not possible to apply a secondary transfer function using Carrara and Ooids standards, as was done with new data, due to insufficient standards having been run during the relevant measurement sessions (Text S2). However, the alignment of the reprocessed Winkelstern data points with new data suggest this is not necessary (Figure 5). Finally,  $\delta^{18}\text{O}_{\text{w}}$  was calculated this time using the mollusk-specific fractionation factor of Grossman and Ku (1986).

#### 2.5. Modern Water Collection and Isotopic and Salinity Analysis

Modern water samples were collected from around the island over two sampling periods and analyzed for  $\delta^{18}\text{O}_{\text{w}}$  for comparison with calculated  $\delta^{18}\text{O}_{\text{w}}$  values from our fossil shells. Eighteen modern water samples were collected from 14 locations around the island: 17 seawater samples, 1 tapwater sample. Tap water in Bermuda comes from underground cisterns beneath each house that collect rainwater falling on the roof and likely approximates weighted annual average composition of local precipitation. Seven water samples were collected in April 2019 and the other 11 were collected in January/February 2020. All nontap water samples were collected near shore, except for the sample near Bird Island, which was collected from a kayak away from shore.

All aqueous samples were first equilibrated with tank  $\text{CO}_2$  gas for at least 48 h and pure, dehydrated  $\text{CO}_2$  was extracted using a custom-built vacuum extraction line (Figure S2; Text S4).  $\delta^{18}\text{O}$  of  $\text{CO}_2$  was analyzed on the same Thermo-Finnegan MAT 253 dual inlet mass spectrometer used for clumped isotopic measurements and  $\delta^{18}\text{O}$  of the original waters through calibrated with in-house liquid standards which, in turn,

**Table 1**  
*Salinity and Isotope Analyses Data for Each Water Sample Collected From Bermuda*

Water sample	Collection date	Water type	Salinity (ppt) <sup>a</sup> (n = 3)	$\delta^{18}\text{O}$ (‰) <sup>b</sup> (n = 2)	Tidal height
South road tap water	April 30, 2019	Tap water	N/A	−3.9	N/A
<b>Northeast</b>					
Cooper's island	January 12, 2020	Seawater	35.6 ± 0.1	+1.2	High tide
<b>Great sound</b>					
Bird island	01 May 2019	Seawater	34.3 ± 0.6	+1.3	High tide
Hamilton	January 11, 2020	Seawater	35.1 ± 0.2	+1.2	
	January 18, 2020	Seawater	35.3 ± 0.8	+1.2	High tide
	January 25, 2020	Seawater	35.1 ± 0.4	+1.3	High tide
	February 01, 2020	Seawater	35.6 ± 0.4	+1.2	Low tide
	February 08, 2020	Seawater	35.0 ± 1.0	+1.3	High tide
Lodge point park	April 29, 2019	Seawater	35.1 ± 0.2	+1.3	Intermediate tide
<b>Outer southwest edge</b>					
Glass beach	February 09, 2020	Seawater	34.5 ± 0.5	+0.9	High tide
Somerset long bay	February 09, 2020	Seawater	34.4 ± 0.6	+1.0	High tide
<b>North shore</b>					
Palmetto roundabout	January 25, 2020	Seawater	34.7 ± 0.8	+1.1	High tide
The flats	January 26, 2020	Seawater	35.1 ± 0.9	+1.1	Intermediate tide
<b>South shore</b>					
Devonshire bay	April 30, 2019	Seawater	35.7 ± 0.4	+1.1	High tide
Elbow beach	January 18, 2020	Seawater	35.7 ± 0.4	+1.8	Low tide
Grape bay	April 29, 2019	Seawater	35.2 ± 1.0	+1.3	Low tide
Hungry bay	April 29, 2019	Seawater	35.5 ± 0.6	+0.8	Low tide
Hungry bay tide pool	April 29, 2019	Seawater	35.7 ± 0.3	+1.3	High tide

<sup>a</sup>Salinity measurements for each sample were replicated at least three times. <sup>b</sup>Errors for  $\delta^{18}\text{O}$  values are reported as long term instrument precision of ± 0.1.

were cross-calibrated using USGS standards (USGS 45, 46). Details of the procedure and a schematic diagram of the extraction line can be found in supplementary material (Figure S2; Text S4).

All water samples were also measured in duplicate for their total salinity using an Extech EC170 salinity meter (Table 1). A third independent salinity measurement was performed using a Leica handheld Temperature Compensated Refractometer for cross-calibration. Basic accuracy for the Extech salinity meter is ±2% and this device reports salinity to 0.1 ppt. The Leica Refractometer has a typical precision of 0.5 ppt. All three measurements were averaged together in Table 1. See supplementary Figure S3 and Table S1 for all data.

### 3. Results

#### 3.1. Isotopic Analysis of Modern Water Samples

Seawater  $\delta^{18}\text{O}_w$  values ranged from  $+0.8 \pm 0.1\text{‰}$  (Hungry Bay) to  $+1.3 \pm 0.1\text{‰}$  (Bird Island; Hamilton; GB; Hungry Bay Tide Pool) (Table 1). The tap water sample had a  $\delta^{18}\text{O}_w$  value of  $-3.9 \pm 0.1\text{‰}$  (Table 1), much lower than all seawater samples.

Seawater samples show a salinity range of 34.2–36.8 psu, as expected (Figure S3). However, no clear correlation between salinity and  $\delta^{18}\text{O}_w$  was observed.

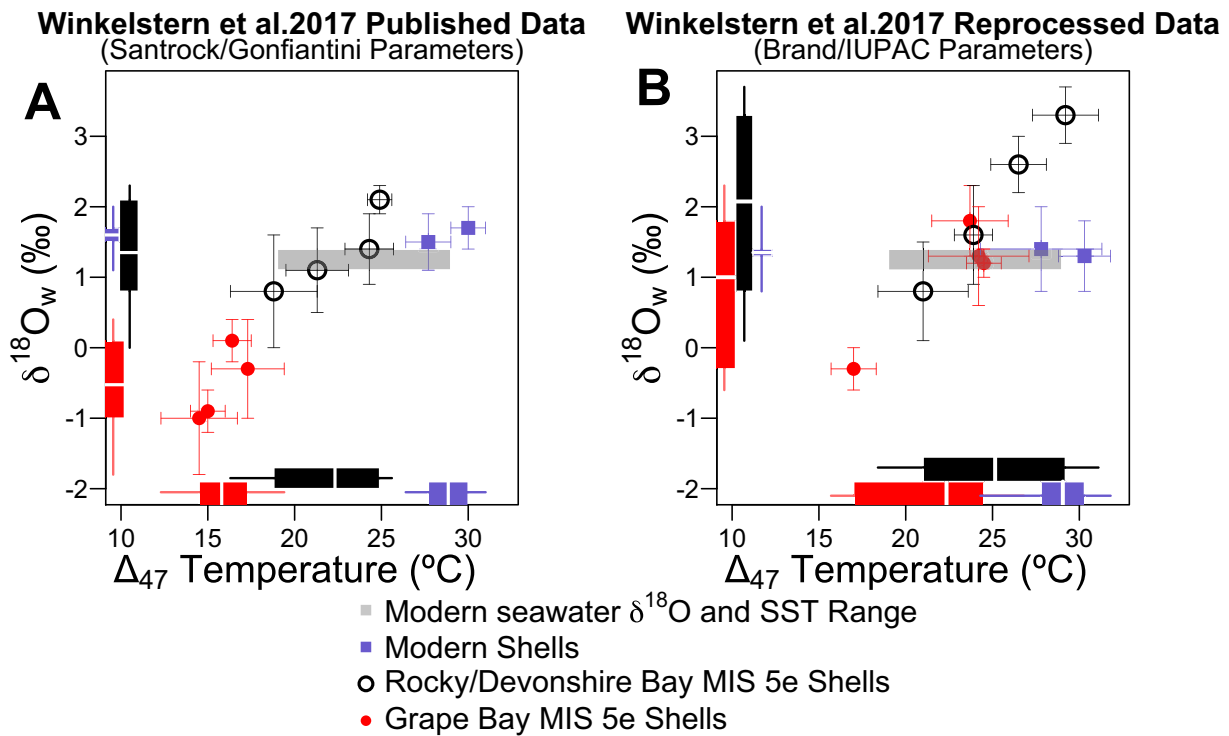


**Figure 2.** Original and reprocessed  $\Delta_{47}$ -temperatures and  $\delta^{18}\text{O}_w$  values from Winkelstern et al. (2017). (a), results as originally published (see text), modified from Figure 3 of original study with added range bars (Winkelstern et al., 2017). Temperatures calculated using Defliese et al., 2015 calibration equation. (b), reprocessed results using updated data processing methods, with temperatures calculated using Brand/IUPAC parameters, synthetic calibration (Petersen et al., 2019) and  $\delta^{18}\text{O}_w$  values calculated using Grossman and Ku (1986) equation. Errors reported for both  $\Delta_{47}$ -temperature and  $\delta^{18}\text{O}_w$  values are based on internal 1 standard error of 3–5 replicates. Gray rectangle denotes modern instrumental variability in temperature (2007–2012 NOAA buoy data) and modern seawater  $\delta^{18}\text{O}$  values (Global Seawater Oxygen-18 Database), as reported by Winkelstern et al. (2017).

### 3.2. Reprocessing of Published Data Using Brand Parameters

Winkelstern et al. (2017) reported  $\Delta_{47}$ -temperatures from GB (15°C–17°C) that were distinct from temperatures calculated for DB/RB (19°C–25°C) (Figure 2a). This finding was puzzling given that the deposits at these sites are apparently coeval and only ~2 km apart (Winkelstern et al., 2017). After reprocessing using Brand/IUPAC parameters with synthetic calibration, the calculated  $\Delta_{47}$ -temperature ranges from the two sites overlap (GB = 17°C–24.5°C; DB/RB = 21°C–29.2°C) (Figure 2b). Except for one GB point, the GB temperatures fall within the DB range (GB range with point removed = 23.7°C–24.5°C).

Reprocessing also decreased differences in calculated  $\delta^{18}\text{O}_w$  values and shifted all  $\delta^{18}\text{O}_w$  values higher. Prior to reprocessing,  $\delta^{18}\text{O}_w$  values from GB were –1 to 0.1‰ and from DB/RB were 0.8–2.1‰ (Figure 2a). After reprocessing, GB  $\delta^{18}\text{O}_w$  values were –0.3 to 1.8‰ and DB/RB  $\delta^{18}\text{O}_w$  values were 0.8–3.3‰ (Figure 2b).

### 3.3. High Resolution Stable Isotope Measurements in the Modern Shell

All three modern shells showed around 3–4 years of growth over the measured interval and demonstrated clear seasonality in  $\delta^{18}\text{O}_{\text{carb}}$  (Figure 3). The seasonal cycle is especially clear in shell BM3 and somewhat distorted in the later part of BM1. Drill points are evenly spaced around the last whorl of the shell and the sample spacing of ~10–15 points per year corresponds to roughly monthly resolution. The pseudo-sinusoidal profiles in the modern shells shown in Figure 3 show an uneven distribution between warmer and cooler seasons. The larger number of points representing the summer months compared to shorter winters indicates variable growth rates throughout the year (faster in summer, slower in winter).

Using the modern water value of +1.16‰, collected from the same sampling location (Cooper’s Island) as the modern *C. pica* shells, we converted the high resolution  $\delta^{18}\text{O}_{\text{carb}}$  values using the mollusk-specific

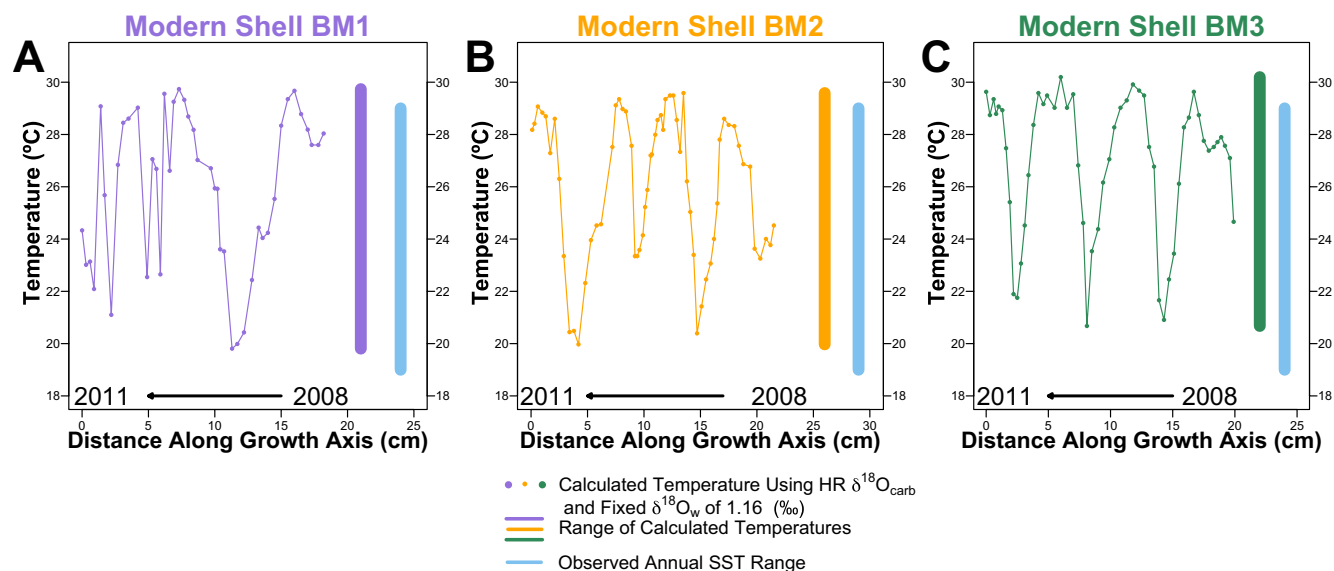


**Figure 3.** Temperature seasonality and range calculated for three modern shells ((a). BM1, (b). BM2, (c). BM3), calculated from high-resolution  $\delta^{18}\text{O}_{\text{carb}}$  profiles using a single  $\delta^{18}\text{O}_{\text{w}}$  value of 1.16‰, selected from modern  $\delta^{18}\text{O}_{\text{w}}$  measurement at collection site, and the mollusk-specific fractionation equation described in Grossman and Ku (1986). Blue bars show instrumental temperature range for comparison.

fractionation equation described by Grossman and Ku (1986) to temperature. Using this  $\delta^{18}\text{O}_{\text{sw}}$  value, our modern shell ranges from 19.8°C to 29.7°C for BM1, 20.0°C–29.5°C for BM2, and 20.7°C–30.2°C for BM3 (Figure 3), compared to the instrumental range of 19°C–29°C. The ranges seen in the three modern shells (BM1 = 9.9°C; BM2 = 9.5°C; BM3 = 9.5°C) match excellently with the observed instrumental seasonal range of 10°C.

In all three modern shells best alignment with modern instrumental temperatures is achieved using the equation described by Grossman and Ku (1986). Therefore, we choose to use Grossman and Ku (1986) equation going forward when calculating  $\delta^{18}\text{O}_{\text{w}}$  values for fossil shells using  $\Delta_{47}$ -based temperatures. A second version of the data calculated using Kim et al. (2007) is available in the supplementary material.

### 3.4. $\Delta_{47}$ and $\delta^{18}\text{O}_{\text{w}}$ Measurements in the Modern Shell BM2

Previously, the modern shell BM2 had been sampled in a single location for  $\Delta_{47}$ , near terminal edge of each shell, reflecting a late summer season temperature based on the high-resolution  $\delta^{18}\text{O}$  profile (Winkelstern et al., 2017). For the current study, 10 additional  $\Delta_{47}$  measurements were made on BM2, targeting the highest and lowest  $\delta^{18}\text{O}_{\text{carb}}$  values to capture the full seasonal range in temperature and  $\delta^{18}\text{O}_{\text{w}}$  to compare with observed temperature and seawater compositions (Figure S1; Figure 4a). The resulting  $\Delta_{47}$  values correspond to temperatures of  $16.1 \pm 3.8^\circ\text{C}$  to  $32.7 \pm 4.4^\circ\text{C}$ , matching well with the observed annual seasonal temperature range (Figure 4b). The average of all BM2  $\Delta_{47}$  measurements is  $23.5^\circ\text{C} \pm 2.6(1\text{sd})$  (include the single measurement from Winkelstern et al., 2017), combining samples from the ~4 years of life represented by the sampled interval (2008–2011). This shows excellent agreement with the observed mean annual temperature of 23°C over the same interval. This close agreement between the  $\Delta_{47}$ -based temperatures and reality indicate *C. Pica* shells do not show any “vital effects” (biologically driven deviations from equilibrium precipitation) in clumped isotope-derived temperatures, or if they do, they are smaller than our measurement error. Fossil *C. pica* shells are therefore likely to be faithful recorders of environmental conditions in  $\Delta_{47}$  as well, as it is unlikely that a species has evolved to have a vital effect over 125,000 years without changing any other physical characteristics defining the species.

$\delta^{18}\text{O}_{\text{w}}$  values were calculated from  $\Delta_{47}$ -based temperatures and co-analyzed  $\delta^{18}\text{O}_{\text{carb}}$ , and using two different equations (Grossman & Ku, 1986; Kim et al., 2007; Figure 4c). Using the Grossman and Ku (1986) equation resulted in a range of  $-1.4 \pm 0.3$  to  $+1.4 \pm 0.9\text{‰}$ , and a mean  $\delta^{18}\text{O}_{\text{w}}$  value of  $0.0\text{‰} \pm 0.5(1\text{sd})$ . Using the Kim et al. (2007) equation resulted in a range of  $-0.5 \pm 0.3$  to  $+2.2 \pm 0.8\text{‰}$ , and a mean  $\delta^{18}\text{O}_{\text{w}}$  value of  $0.9\text{‰} \pm 0.5$



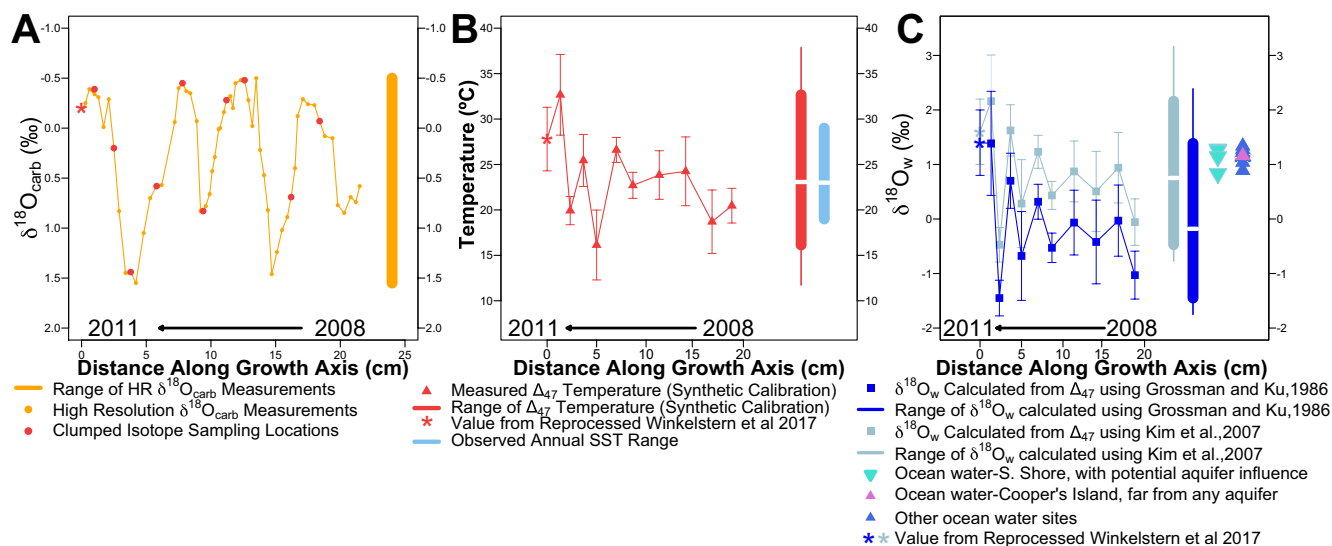


**Figure 4.** (a), High-resolution  $\delta^{18}\text{O}_{\text{carb}}$  profile from modern shell BM2, with clumped sampling locations shown in red. (b), Subannual  $\Delta_{47}$ -based temperatures from modern specimen BM2. Full measured range is plotted compared to modern instrumental range on the right (blue). (c), Subannual  $\delta^{18}\text{O}_w$  calculated from  $\Delta_{47}$ -based temperatures and co-analyzed  $\delta^{18}\text{O}_{\text{carb}}$ , using two different equations (Grossman & Ku, 1986; Kim et al., 2007). Measured range in  $\delta^{18}\text{O}_w$  plotted on the right side compared to  $\delta^{18}\text{O}_w$  values measured on modern waters. Errors reported for both  $\Delta_{47}$ -temperature and  $\delta^{18}\text{O}_w$  values are 1 standard error.

(1sd). The measured value at Cooper's Island plots within error of the mean  $\delta^{18}\text{O}_w$  value calculated using the Kim et al. (2007) equation, and is within both measured  $\delta^{18}\text{O}_w$  ranges. The calculated  $\delta^{18}\text{O}_w$  values from both equations yield greater than expected ranges (2.8‰ for all points included), given the previous (and commonly used) assumption that  $\delta^{18}\text{O}_w$  is seasonally invariant (Winkelstern et al., 2017). However, modern seawater samples from around the island display a nonzero range in  $\delta^{18}\text{O}_w$  (+0.8 to +1.3‰ for a range of 0.5‰) (Figures 4c and 5b).

### 3.5. $\Delta_{47}$ and $\delta^{18}\text{O}_w$ in Fossil Shells

Fossil shells were sampled in four additional positions for clumped isotopes, selected to target the high and low  $\delta^{18}\text{O}_{\text{carb}}$  values.  $\Delta_{47}$  values from GB shells recorded temperatures of 10.1°C–24.5°C, and a  $\delta^{18}\text{O}_w$  range of −2.1 to +1.8‰ (Figure 5).  $\Delta_{47}$  in DB/RB shells recorded temperatures of 12.7°C–35.2°C, with a  $\delta^{18}\text{O}_w$  range of −2.03 to +3.3‰ (Figure 5). The larger temperature range observed in DB/RB is driven primarily by one sample with a temperature of 35.2°C, 6°C higher than the next closest sample from either fossil site. With this one point removed, temperature range for DB reduces to be 12.7°C–29.2°C, matching much more closely with GB.

DB/RB and GB shells show minimum temperatures colder than both the modern shell and modern observations, but the overall temperature range is comparable. The fossil shells have a range of 25.2°C ( $10.1 \pm 5.5^\circ\text{C}$  to  $35.2 \pm 7.0^\circ\text{C}$ ) or a reduced range of 19°C with the highest points removed. The modern shell has a range of 16.6°C ( $16.1 \pm 3.8^\circ\text{C}$  to  $32.7 \pm 4.4^\circ\text{C}$ ) compared to modern instrumental data which records a range of 10°C (from 19°C to 29°C, monthly means) (Figure 5). Shells from both fossil sites show a wider range in  $\delta^{18}\text{O}_w$  than the modern shells, potentially due to their proximity to the central lens aquifer (discussed below).

## 4. Discussion

### 4.1. Assessing the Validity of Isotopic Proxies in *Cittarium pica* Using a Modern Shell

#### 4.1.1. Stable Isotope Patterns

$\delta^{18}\text{O}_{\text{carb}}$  is a function of both temperature and the isotopic composition of water ( $\delta^{18}\text{O}_w$ ) (Epstein et al., 1953), both of which have the potential to change on annual timescales. High resolution measurements of  $\delta^{18}\text{O}_{\text{carb}}$

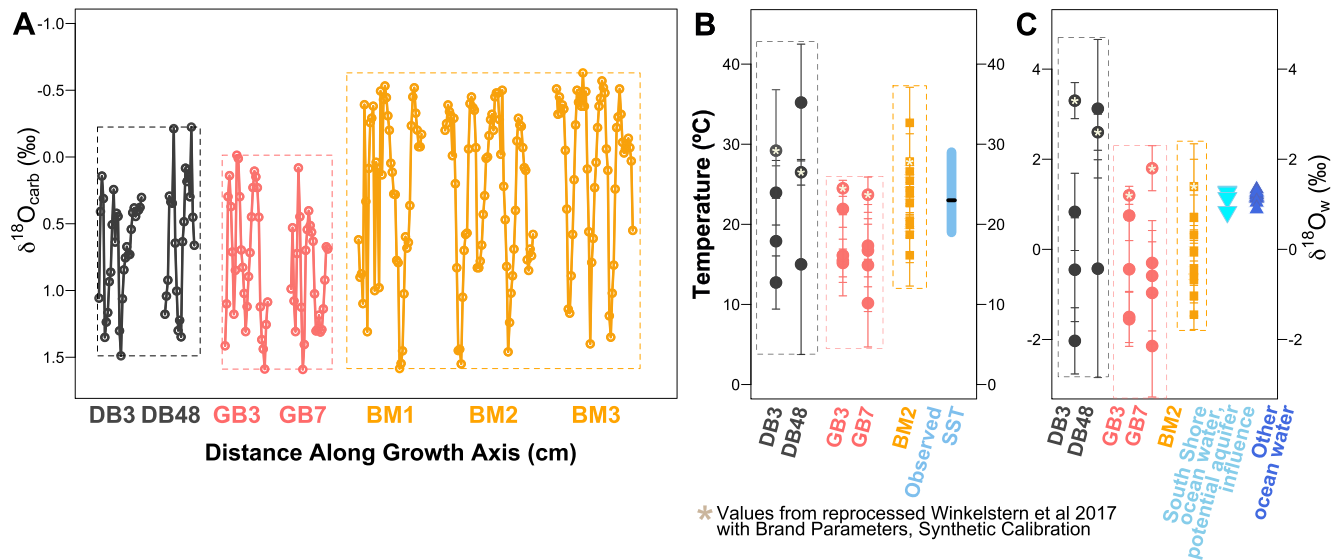


**Figure 5.** (a), High Resolution  $\delta^{18}\text{O}_{\text{carb}}$  profiles from fossil and modern shells with ranges indicated by encompassing boxes. (b),  $\Delta_{47}$ -derived temperatures and temperature ranges of fossil and modern shells compared to modern sea surface temperature (SST). (c),  $\delta^{18}\text{O}_w$  values and ranges of fossil and modern shells, calculated using Grossman and Ku (1986) mollusk-specific fractionation equation, compared to measured modern  $\delta^{18}\text{O}_w$  values on the right. Errors reported for both  $\Delta_{47}$ -temperature and  $\delta^{18}\text{O}_w$  values are based on 1 standard error.

in *C. pica* show sinusoidal, apparently annual cycles, suggesting that shells of this species seemingly can record annual climate fluctuations, albeit with a heavier weighting toward the summer months. When  $\delta^{18}\text{O}_w$  is assumed to be invariant and equal to the value measured for seawater at the collection locality at Cooper's Island (1.16‰), the calculated  $\delta^{18}\text{O}_{\text{carb}}$ -based temperature range using the mollusk-specific fractionation equation described by Grossman and Ku (1986) is 19.8–30.2°C for the three shells combined (Figure 3), which matches well with the observed range of 19–29°C from NOAA National Data Buoy Center (<https://www.ndbc.noaa.gov/>). We do not have year-round water sampling at Cooper's Island to directly confirm low variability in  $\delta^{18}\text{O}_w$  over the lifespan of the calibration shells, but the close agreement between  $\delta^{18}\text{O}_{\text{carb}}$ -based temperature range assuming invariant  $\delta^{18}\text{O}_w$  and the instrumental temperature range, as well as the sinusoidal shape of the  $\delta^{18}\text{O}_{\text{carb}}$  record, suggests that temperature is the primary driver of the observed variations in  $\delta^{18}\text{O}_{\text{carb}}$  in the modern Cooper's Island shell.

However, this conclusion does not immediately apply to all *C. pica* shells. It is possible that variations in  $\delta^{18}\text{O}_w$  could occur, now or in the past, at other locations around the island. Modern seawater  $\delta^{18}\text{O}_w$  measurements indicate variations of  $\sim 0.5\text{‰}$  are possible throughout the year and variations of  $0.3\text{‰}$  are possible from a single location (Hamilton) over a span of weeks (Table 1, Figure 4c). Instead, this is meant to indicate that no significant vital effects in  $\delta^{18}\text{O}_{\text{carb}}$  are present that would distort environmental signals in *C. pica* shells.

#### 4.2. MIS 5e in Bermuda Cooler Than Modern

Combining 2–4 new subannual-scale measurements with reprocessed data from Winkelstern et al. (2017) (1/shell) results in 3–5  $\Delta_{47}$  samples per fossil shell, selected to cover the full seasonal range in temperature. These samples should, when averaged together, more accurately capture mean annual conditions compared to the single  $\Delta_{47}$  sample previously published per shell. Shell averages in the DB/RB and GB fossil shells range from 16.6°C to 25.6°C, this is colder than the average temperature recorded by  $\Delta_{47}$  in the modern shell BM2 (23.5°C), which accurately captures modern mean annual temperature of 23°C, indicating temperatures in Bermuda during MIS 5e were cooler than today (Figure 5). This result agrees with foraminiferal faunal analog-based regional patterns of reconstructed MIS 5e SSTs that show Bermuda to be cooler than modern by 5°C (CLIMAP, 1984; Turney & Jones, 2010) and is consistent with the major conclusion previously made by Winkelstern et al. (2017).

Other studies have suggested the presence of *C. pica*, a generally warm-water species, in MIS5e deposits indicates climates must have been warmer than modern during the Last Interglacial, citing the absence of this species in modern Bermuda but its presence in warmer regions to the south (Muhs et al., 2002). However, since collection bans were put in place, populations of *C. pica* have flourished in Bermuda in recent years. For example, *C. pica* shells were live-collected (with a permit) in 2014 for isotope analysis (Winkelstern et al., 2017) and were observed by the authors in abundant numbers on the rocky shores of Hungry Bay in 2019, indicating additional factors beyond temperature likely influence their success. Olson and Hearty (2013), after finding *C. pica* fossils in marine deposits in Bermuda dating to MIS 7, 9, and 11, argue that *C. pica* was expatriated in each glacial period and re-colonized Bermuda four separate times over the past ~200,000 years. This conclusion assumes that *C. pica* could not tolerate the colder temperatures of glacial intervals. However, marine units equivalent to those in which *C. pica* fossils are found are not preserved on the island of Bermuda during glacial times due to much lower sea level and the authors state that no marine gastropods of any kind were found in the terrestrial deposits they searched (Olson & Hearty, 2013), but it is unlikely that all species were wiped out and re-colonized each glacial cycle. Therefore, we conclude that faunal analog arguments are fraught here, as there are no equivalent facies during colder periods in which to observe the presence or absence of fossils, and stronger conclusions can be based on isotopically derived absolute temperatures like those presented here.

Unlike Winkelstern et al. (2017), however, we observed no systematic temperature differences between the two study sites in new data or reprocessed published data (Figures 2 and 5). As originally published, GB temperatures were 10°C cooler and  $\delta^{18}\text{O}_w$  values 0.7‰ lower than modern, and were hypothesized to record a meltwater event delivering cold and isotopically depleted freshwaters all the way from Greenland. Exact ages of Devonshire Marine Member deposits at GB and DB/RB are overlapping, but not identical (see Winkelstern et al., 2017 Figure 5). The potential for GB deposits to possibly represent the beginning of the cooler phase MIS5d was previously used to explain anomalously cold temperatures from those shells. In the new and reprocessed data, fossil shells from both sites record similar temperatures and  $\delta^{18}\text{O}_w$  values, eliminating the need for explanations as to why they differed despite being close together and the same age (Figures 2 and 5). Further, since the apparent temperature difference between the two sites is resolved here, this lends additional support to the interpretation of the two deposits as being of the same age. Given the measured age ranges for both (Harmon et al., 1983; Muhs et al., 2002), this suggests the common age range of 120–126 ka, during peak warmth of MIS5e.

### 4.3. Unexpectedly Large Subannual Variations in $\delta^{18}\text{O}_w$ Recorded in Fossil Shells

Typical sclerochronology studies convert high-resolution  $\delta^{18}\text{O}_{\text{carb}}$  records into subannual temperature records by assuming a constant  $\delta^{18}\text{O}_w$  value and calculating a single temperature value for each  $\delta^{18}\text{O}_{\text{carb}}$  data point (Buick & Ivany, 2004; Burchell et al., 2013; Hallmann et al., 2008; Schöne et al., 2004; Wanamaker et al., 2008; Winkelstern et al., 2013). In this scheme,  $\delta^{18}\text{O}_{\text{carb}}$  values increase as temperatures cool, and vice versa, according to the temperature dependence of  $\delta^{18}\text{O}_{\text{carb}}$  established in laboratory calibration studies (e.g., Grossman & Ku, 1986). By measuring  $\Delta_{47}$ -based temperatures at the subannual scale,  $\delta^{18}\text{O}_w$  is instead allowed to vary throughout the year and we can establish a subannual record of temperature independent of  $\delta^{18}\text{O}_w$ .

Our subannual clumped isotope measurements on all four fossil shells demonstrated an unexpected, inverse relationship between  $\delta^{18}\text{O}_{\text{carb}}$  and temperature. We find the coldest  $\Delta_{47}$ -derived temperatures correspond to the lowest, not highest,  $\delta^{18}\text{O}_{\text{carb}}$  values (Figure 6). This inverse relationship necessarily results in calculated  $\delta^{18}\text{O}_w$  values that vary significantly over the year, in an out-of-phase relationship with temperature. We therefore observe low  $\delta^{18}\text{O}_w$  values corresponding to the coldest times and high  $\delta^{18}\text{O}_w$  values during warmer times. The range in  $\delta^{18}\text{O}_w$  values within one shell is >2‰, indicating unexpectedly large variation in coastal  $\delta^{18}\text{O}_w$ .

Given the sampling resolution (2 pts/year, each averaging ~1–2 months), the >2‰ range in  $\delta^{18}\text{O}_w$  recorded by the fossil shells reflects seasonal-scale, as opposed to inter-annual, variability. The paleoenvironment in which the MIS 5e shells lived is thought to be very similar to the current South Shore environment seen at Hungry Bay – an unencumbered, rocky shoreline facing out into the Atlantic on a small carbonate platform with no surface rivers, well mixed by wave action. This makes it seemingly difficult to explain such large variations

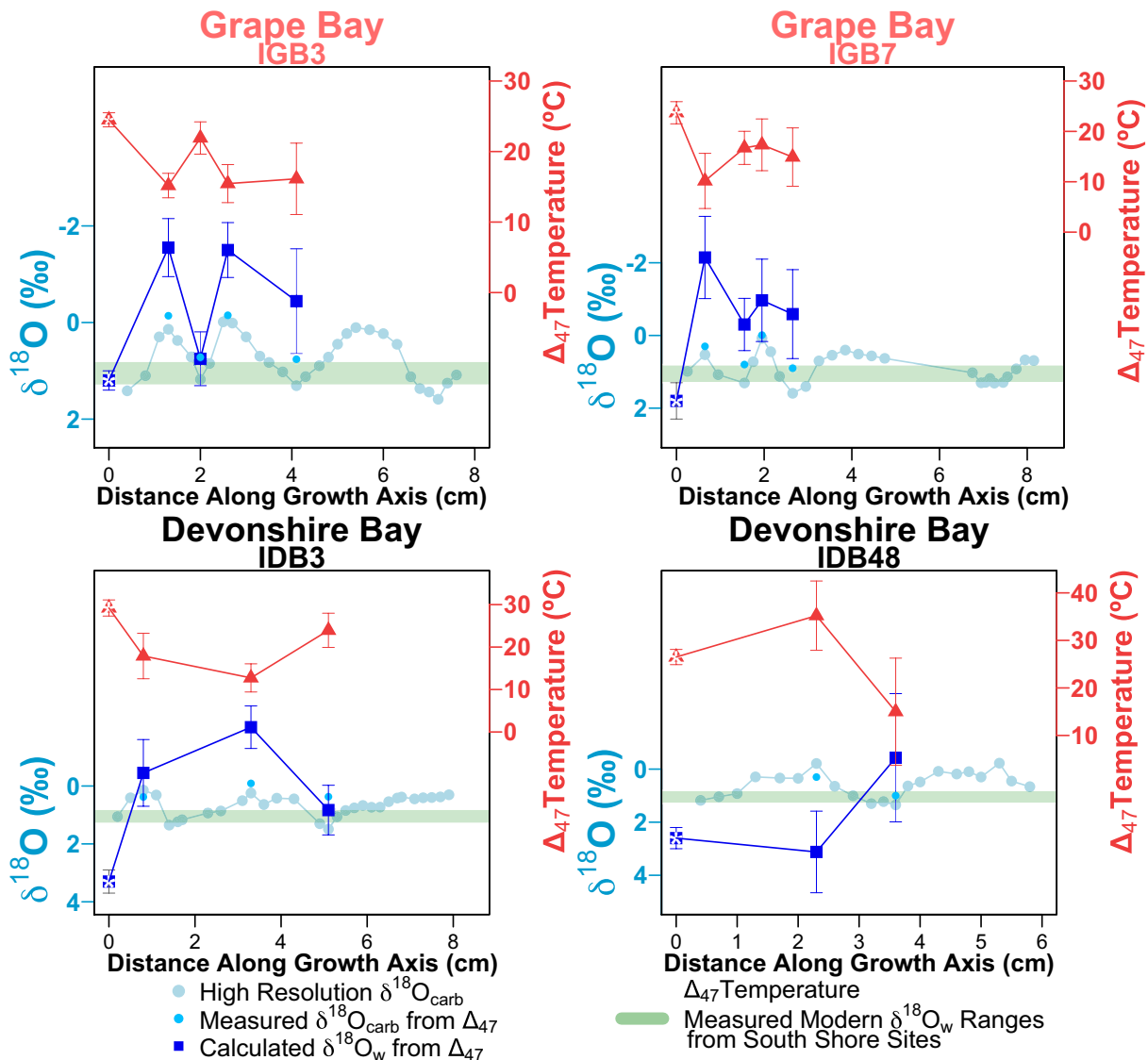


**Figure 6.** High resolution and bulk  $\delta^{18}\text{O}$  measurements,  $\Delta_{47}$ -based temperatures and  $\delta^{18}\text{O}_w$  values, calculated using Grossman and Ku (1986) aragonite-water equilibrium equation, for four fossil shells compared to modern  $\delta^{18}\text{O}_w$  variability. Note that the y-axes are scaled differently in each plot for best visibility of overlapping data.

in  $\delta^{18}\text{O}_w$ , as wave action would be expected to dilute away any isotopic anomalies into surrounding seawater. *C. pica* shells live on rocky substrates below the high-tide line, but are often exposed or partially exposed during low tide. Any isotopic gradients produced by the injection of freshwater would therefore need to be maintained only in this extremely near-shore environment and do not necessarily need to extend far offshore.

In the following sections, we explore multiple possible mechanisms that could result in the large changes in coastal seawater  $\delta^{18}\text{O}_w$  we observed in our fossil data and use modern water samples and modern shell data to distinguish between these mechanisms.

#### 4.3.1. Propagation of Uncertainty

Modern  $\delta^{18}\text{O}_w$  around Bermuda only varies over a small range (0.5‰ total, 0.2‰ within a given region excluding south shore), but the modern shell BM2 shows a bigger range in  $\delta^{18}\text{O}_w$  values calculated from  $\Delta_{47}$ -based temperatures and  $\delta^{18}\text{O}_{\text{carb}}$  values. No measurements exist documenting the true range in  $\delta^{18}\text{O}_w$  at Cooper's island throughout the year, but it's unlikely to be much bigger than the total island variability

of 0.5‰. The large range in  $\delta^{18}\text{O}_w$  values reconstructed from modern shell BM2 might be because of pseudo-propagation of uncertainty - that the relatively large uncertainty in  $\Delta_{47}$ -based temperatures leads to an amplified range in calculated  $\delta^{18}\text{O}_w$  values (Note: This is not the same as actual propagation of uncertainty where error on temperature is mathematically transferred through calculation of  $\delta^{18}\text{O}_w$ ).

In the case of the modern shells, converting  $\delta^{18}\text{O}_{\text{carb}}$  values to temperature using a fixed  $\delta^{18}\text{O}_w$  value and the aragonite temperature relationship of Grossman and Ku (1986) correctly captures the seasonal temperature range (Figure 3). In BM2,  $\Delta_{47}$ -based temperatures overestimate the seasonal range, yet still got the mean temperature correct (Figure 4b). However, the hottest/coldest temperatures do not always align with the lowest/highest  $\delta^{18}\text{O}_{\text{carb}}$  values, leading to more divergent  $\delta^{18}\text{O}_w$  values. Supporting this pseudo-uncertainty propagation theory for the expanded range in  $\delta^{18}\text{O}_w$  in the modern shell, the variability in  $\delta^{18}\text{O}_w$  does not correlate with  $\delta^{18}\text{O}_{\text{carb}}$  in BM2 (Figure 4).

In the fossil shells, the situation is different. The pattern of variability is aligned with  $\delta^{18}\text{O}_{\text{carb}}$  variation, in all four shells with the exception of the middle point on DB48, which we have already identified as an outlier for being higher than reasonable temperature (see 3.5). Therefore, even though the same pseudo-propagation of errors may be artificially amplifying the variation in fossil  $\delta^{18}\text{O}_w$ , the pattern of variation is potentially indicating real environmental variations in  $\delta^{18}\text{O}_w$  on a seasonal scale.

#### 4.3.2. Highly Seasonal Precipitation

One possible source of variation in  $\delta^{18}\text{O}_w$  is precipitation-driven surface runoff transiently depleting coastal  $\delta^{18}\text{O}_w$ . Bermuda has an average annual precipitation of 1,468 mm which is fairly evenly distributed throughout the year, with slightly more rainfall in summertime (Rowe, 1984). Monthly average precipitation rates range from 75 to 172 mm (Rowe, 1984). Precipitation  $\delta^{18}\text{O}$  in Bermuda, as elsewhere, is much lower relative to seawater, best indicated by the  $-3.9\text{‰}$  tap water sample which approximates the annual average isotopic composition of local precipitation as tap water in Bermuda comes from underground cisterns beneath each house that collect rainwater falling on the roof. Since Bermudian tap water, and therefore precipitation, has a much lower  $\delta^{18}\text{O}_w$  value than local seawater (average of  $1.2\text{‰}$  for 17 seawater samples), surface runoff of precipitation (or direct rainout on surface waters) could reduce  $\delta^{18}\text{O}_w$  during times of increased precipitation.

This phenomenon is possibly observable in the modern shell BM2. In the four years the sampled shell lived (2008–2011), there was one month with anomalously high precipitation – June 2009 (LDEO Climate Group Datasets) (Figure S4). This appears to align with a single-point spike in the high resolution  $\delta^{18}\text{O}_{\text{carb}}$  record of shell BM2, slightly before the 2009 summertime peak (Figure S4). However, no anomaly in  $\delta^{18}\text{O}_{\text{carb}}$  is seen in BM1 or BM3, making us hesitant to interpret based on a single (unreplicated) measurement. If real, this offset from the expected temperature-driven sinusoid is on the order of  $0.75\text{‰}$  (Figure S4), and is so transient as to be completely missed in 2 of 3 shells at our  $\sim$ monthly (to sub-monthly in summer) sampling resolution (Figure 3). This constrains the order of magnitude and duration of a potential precipitation-driven change in  $\delta^{18}\text{O}_w$ , and indicates that the extent of influence of precipitation changes on  $\delta^{18}\text{O}_w$  determined from fossil samples should be minimal. Further, based on instrumental precipitation records, the month of highest precipitation can occur in different summertime months, and some years have no anomalously high rainfall months at all (e.g., 2008 and 2011). Other less extreme rainy months (e.g., September 2010) were absent in all three modern shells, indicating that for precipitation to impact  $\delta^{18}\text{O}_w$ , rainfall must be significantly above background levels.

In contrast, variations in  $\delta^{18}\text{O}_w$  seen in fossil shells are greater in magnitude ( $>2\text{‰}$  within a single shell, although this may be amplified by an unknown amount) and, more importantly, seem to vary seasonally and in every year measured (excluding the one high point in DB48). We see two single-point spikes in the high resolution  $\delta^{18}\text{O}$  profile of shell DB48, which could reflect especially rainy periods, but these are very short (Figure 5). One of these spikes corresponds to the middle sample that has been potentially identified as an outlier due to its elevated temperature of  $>35^\circ\text{C}$ . However, the  $\delta^{18}\text{O}_{\text{carb}}$  value measured during clumped isotope analysis was lower and more in line with adjacent points, potentially indicating a measurement error in the original high-resolution profile.

If the observed  $\delta^{18}\text{O}_w$  variability in our four fossil shells was driven by changes in precipitation-driven surface runoff, it would require rainfall levels potentially more than twice as high as the rainiest months today,

occurring every summer season. We would also expect precipitation-driven effects on  $\delta^{18}\text{O}_w$  to be similar everywhere around the island. Fossil *C. pica* shells are primarily found along the south shore due to their preference for a rocky habitat. Future studies looking at MIS 5e-aged shells (of necessity sampling different species) collected from other locations around the island, would help validate or refute this potential mechanism.

#### 4.3.3. Coastal Upwelling

Variability in coastal  $\delta^{18}\text{O}_w$  could be affected by coastal upwelling. Typically, coastal water show significant variability as depth increases, and upwelling holds extreme importance in mixing water from different depth columns and maintaining productivity (Jacob et al., 2016; Killingley & Berger, 1979; Tao et al., 2013). Further, strong seasonal-wind-driven upwelling could bring cold,  $^{18}\text{O}$ -enriched, nutrient-rich water to the surface resulting in higher  $\delta^{18}\text{O}$  values (Jacob et al., 2016; Killingley & Berger, 1979; O'Dea et al., 2007; Tao et al., 2013). Mainly driven by seasonal wind, its intensity also changes seasonally. There are no measurements of  $\delta^{18}\text{O}_w$  value of the deep water in order to determine the potential of this mechanism to affect coastal surface  $\delta^{18}\text{O}_w$  values. However, the size of this effect can be estimated by looking at salinity variation with depth, as salinity and  $\delta^{18}\text{O}_w$  often correlate strongly within a region due to similar controlling processes. Salinity profiles from Hydrostation S, an offshore long-term monitoring site run by the Bermuda Biological Station, recorded minimal salinity variation from the upper column (0–10m) down to 2000 m (36.6 psu to 35 psu, respectively) (<https://www.st.nmfs.noaa.gov/copepod/time-series/us-10102/>). This salinity profile suggests that deep waters likely have similar  $\delta^{18}\text{O}_w$  values to surface waters around Bermuda. Therefore, variable contribution of deep water is unlikely to cause large variations in coastal  $\delta^{18}\text{O}_w$  today. For this mechanism to explain large variations in coastal  $\delta^{18}\text{O}_w$  in the past, coastal upwelling must have been stronger or deep water off Bermuda must have been more isotopically different than today. Future measurements of the  $\delta^{18}\text{O}_w$  value of modern deep waters and microfossils from offshore MIS5e sediments would help constrain whether this mechanism could be responsible for coastal  $\delta^{18}\text{O}_w$  variability during the Last Interglacial.

#### 4.3.4. Subsurface Discharge From the Central Freshwater Lens

The proximity of our fossil sites to the largest of four freshwater aquifers in Bermuda (Devonshire lens; Figure 1) may provide a potential explanation for the large variations seen in  $\delta^{18}\text{O}_w$ . Freshwater from aquifers is injected into near-coastal waters via the subsurface, with discharge rates controlled by aquifer fill rates (i.e., local precipitation rates), topographic gradients, subsurface porosity, and sea level height at the coast (Vacher, 1978). Freshwater in these aquifers is sourced from local precipitation, which has a composition significantly different than seawater (approximated as  $-3.9\text{‰}$  from local tap water, compared to  $\sim 0.8\text{--}1.3\text{‰}$  in seawater samples), meaning that increased subsurface aquifer discharge could reduce coastal  $\delta^{18}\text{O}_w$  values and salinities.

Increased subsurface discharge could be induced by increased recharge into the aquifers (i.e., increased precipitation) or due to a drop in coastal sea surface height. In the case of increased recharge, this would act similarly to the surface runoff mechanism described above. During periods of heavy rain, the subsurface water table height would temporarily rise, leading to more discharge at the coast as the lens returned to equilibrium, decreasing coastal  $\delta^{18}\text{O}_w$  values. However, as above, this would likely be transient, caused by individual storms or stormy weeks/months, with a possible time lag for the gradient imbalance to travel through the aquifer. In order for this to explain our data, very heavy rainfall would have to occur every winter, unlike today, when peak rainfall typically occurs in summer.

On the other hand, three processes contribute to systematic and predictable changes in coastal sea surface heights: 1) semi-diurnal astronomical tides ( $\sim 0.7\text{--}0.9$  m); 2) daily to weekly isostatic effects from changes in atmospheric pressure ( $\sim 0.2$  m); 3) seasonal thermal expansion ( $\sim 0.6$  m), induced by seasonal warming and cooling of North Atlantic ocean temperatures (Rowe, 1984; Vacher, 1978). During periods of high sea level (either high tide, or late summer after maximum thermal expansion), ocean water would act as a dam, blocking the aquifer from discharging as much freshwater, resulting in higher, more marine  $\delta^{18}\text{O}_w$  values. When sea surface heights were lower (low tide or end of winter), the topographic gradient between the center of the island/aquifer and coastal waterline would increase, causing increased discharge from the

freshwater lens and resulting in lower coastal  $\delta^{18}\text{O}_w$  values due to an increased component of isotopically depleted aquifer water (Rowe, 1984; Vacher, 1978).

Evidence for tidally driven subsurface discharge has been observed in Bermuda today. In Green Bay Cave on the north side of the island, daily tidal flow mixes freshwater out into coastal seawater, causing documented changes in salinity (and presumably in  $\delta^{18}\text{O}_w$  as well, although it hasn't been measured) (van Hengstum & Scott, 2012). Tidally driven subsurface discharge also occurs in other areas with coastal carbonate aquifers such as the Bahama Bank (Beddows et al., 2007; Moore, 1996; Vacher & Wallis, 1992; Whitaker & Smart, 1990).  $\Delta_{47}$ -based  $\delta^{18}\text{O}_w$  values measured in our fossil shells show changes on the seasonal-, not tidal-, scale. This could be achieved through a similar mechanism, driven by thermal expansion instead of daily tides. Thermal expansion causes mean sea level heights to fluctuate at nearly the same magnitude as daily tides, but on the months-to-year timescale suggested by the fossil data. Sea surface heights increase throughout the summer as surface waters warm and expand, peaking in September/October, some of the warmest months (Figure S8). Lowest sea surface heights occur in February/March, aligning with the coldest months of the year (Figure S8). In this way, higher aquifer discharge (and therefore lower  $\delta^{18}\text{O}_w$  values) could align with the colder months. Slight misalignment between peak temperatures (JAS) and maximum sea surface heights (SON) may explain the reduced apparent seasonal amplitude in fossil shells compared to modern (Figure 5).

This mechanism could potentially apply to any stretch of coastline proximal to one of the four major subsurface aquifers on Bermuda (Figure 1), but is perhaps most likely to play a role along the South Shore, where our fossil samples were collected. High permeability in the Belmont Formation outcropping along the South Shore makes this stretch of coast more likely to experience higher levels of freshwater discharge than locations on the north shore equally close to the Devonshire aquifer (Vacher, 1978). Freshwater outflow has not been previously documented in this region, but clumped isotopic measurements of marine cements indicate the presence of isotopically depleted waters in the coastal subsurface. Marine cements from along the South Shore record  $\delta^{18}\text{O}_w$  values mostly between  $-3.8$  and  $+3.9\text{‰}$ , with a few even lower than  $-5\text{‰}$  (Defliese & Lohmann, 2016).

#### 4.4. Present-Day Tidal Variability in $\delta^{18}\text{O}_w$ as a Proxy for Past Seasonal Variability

In April 2019 and January-February 2020, seawater samples were collected from around the island, spanning multiple tidal heights. Absolute  $\delta^{18}\text{O}_w$  values differed between regions, but within most regions, measured  $\delta^{18}\text{O}_w$  values were tightly clustered and inter-regional differences could be explained by geography. Samples from the outer southwest edge of the island were lower (GLB and SLB;  $0.9\text{--}1.0\text{‰}$ ) compared to samples from north shore (TF, PR =  $1.1\text{‰}$ ) and Great Sound (BI, H1-5, LPP,  $1.2\text{--}1.3\text{‰}$ ) (Table 1). High  $\delta^{18}\text{O}_w$  values found in samples from the Great Sound are consistent with higher evaporative enrichment in this semi-enclosed basin. Unlike all other collection sites which face out to the open Atlantic Ocean, the Great Sound forms a natural harbor within the curve of the island, surrounded on all sides by land except for the northeast, where it is open to a shallower region of the Atlantic Ocean overlying a submerged Bermuda platform. Lower values in other regions may reflect proximity to freshwater lenses (e.g., SLB and the Somerset Lens) (Figure 1). The variability seen within each of these regions is at the level of measurement error ( $\pm 0.1\text{‰}$ ), consistent with regionally homogenous and constant seawater compositions, regardless of tidal height. Particularly, five measurements from the same location in the capital city of Hamilton over a period of 2 months show variability of  $<0.2\text{‰}$  despite spanning multiple tidal heights. In contrast, the full magnitude of across-island variability was realized in samples collected from a single region – the South Shore. Here, modern seawater  $\delta^{18}\text{O}_w$  values ranged from  $0.8$  to  $1.3\text{‰}$ , and variability was related to tidal height (Figure S10, Table 1).

The relationship between  $\delta^{18}\text{O}_w$  and sea surface height is best demonstrated by two samples from Hungry Bay. There, the seawater samples collected as the tide was rising from its minimum (Table 1, Figures S9 and S10) recorded a lower value of  $0.8\text{‰}$ , while at the same location at the same time, water from a stranded tide pool recorded a value of  $1.3\text{‰}$ , likely representing the composition of seawater during the preceding high (and lowering tide: Figures S9 and S10). Water collected at high tide from Devonshire Bay had a  $\delta^{18}\text{O}_w$  value of  $1.1\text{‰}$ , reflecting a higher isotopic value consistent with a lower freshwater contribution (Figure S10b). However, other low-tide samples from both GB and EB ( $1.3$  and  $1.2$ ) show high values as

well, seemingly in poor agreement with our proposed mechanism. These sites are both located farther away from the Devonshire Lens than DB and HB (Figure 1) and rocky cliffs that must have been present during MIS 5e to support *C. pica* shells have been replaced with sandy beaches at these sites, potentially impacting permeability and reducing freshwater discharge. In contrast, both DB and HB still have rocky shorelines and support modern populations of *C. pica*, making these sites more representative of the MIS 5e environment. Regardless of the timing and  $\delta^{18}\text{O}_w$  values from individual sites, it is clear that the largest variability in  $\delta^{18}\text{O}_w$  within one region and the lowest absolute value (0.8‰) exists along the South Shore, consistent with freshwater discharge mechanisms. Additionally, the next lowest values are found in the southwestern region (0.9–1.0‰), which is also close to a freshwater lens (Somerset Lens), and may be similarly influenced by subsurface freshwater.

Our samples were mostly collected from off-peak tidal times, it is possible the true range in  $\delta^{18}\text{O}_w$  values would increase with a higher sample frequency specially designed to capture both extremes within a tidal cycle. Sea level changes during tidal cycles (0.6 m) compare to the annual, thermal-expansion-driven, cycle (1m), implying a similar magnitude change in  $\delta^{18}\text{O}_w$  could be expected throughout one year. Future work will be required to track  $\delta^{18}\text{O}_w$  variability around the island on the annual scale to compare to the timescales recorded in fossil shells.

#### 4.5. Implications for MIS5e Bermuda

Overall, our fossil data shows very large changes in  $\delta^{18}\text{O}_w$ , and we present a number of hypotheses to explain this data. Larger-than-expected variation in calculated  $\delta^{18}\text{O}_w$  in the modern shell indicates that this subannual clumped isotope approach may overestimate the range in  $\delta^{18}\text{O}_w$  values when temperature extremes do not align with  $\delta^{18}\text{O}_{\text{carb}}$  extremes. However, even if the amplitude of the effect is overestimated, coherent patterns of low/high  $\delta^{18}\text{O}_w$  values during winter/summer seasons demand explanation.

If precipitation were to drive these anomalies, it would require extreme wintertime precipitation every year, contradictory to the modern climatology which has peak rainfall in summer. If coastal upwelling were to drive observed variability in fossil shells, deep waters during MIS 5e must have been isotopically very different from surface waters, unlike gradients today indicated by salinity. We therefore conclude that a freshwater discharge mechanism, driven by changes in sea surface height, is the most likely explanation, as the isotopic composition of that freshwater is significantly different from seawater (−4‰ vs. +1‰) and the largest variability in modern coastal  $\delta^{18}\text{O}_w$  is observed along the South Shore today, proximal to the largest freshwater lens under the island. Thermal expansion changes sea surface heights on seasonal timescales, with peak heights, and therefore most marine  $\delta^{18}\text{O}_w$  values, occurring in late summer/fall coinciding with some of the warmest months.

This suggests that a freshwater lens likely existed under the island of Bermuda during MIS 5e in a similar location to the central lens today and variably ejected freshwater into the South Shore coast region on an annual scale, leading to measurable annual-scale variations in  $\delta^{18}\text{O}_w$ .

## 5. Conclusions

Previous data reconstructing conditions in Bermuda during the Last Interglacial showed divergent temperatures from two closely spaced and apparently coeval sites. Reprocessing this published data and combining it with new subannual-resolution clumped isotope measurements bring both sites into alignment and into agreement with established records in showing cooler-than-modern temperatures in Bermuda during MIS 5e. Although the small number of shells studied (4 fossils) should be accompanied by caveats about representativeness of longer-term average climate, the close agreement between absolute temperatures and temperature ranges across these four shells from two localities is encouraging. All four shells have average temperatures cooler than modern.

Additionally, subannual measurements revealed large (>2‰) seasonal variations in  $\delta^{18}\text{O}_w$ , occurring out of phase with seasonal temperature changes. This magnitude may be amplified by misalignment between extrema in  $\delta^{18}\text{O}_{\text{carb}}$  and  $\Delta_{47}$ -temperatures, propagated through calculations of  $\delta^{18}\text{O}_w$ , as seen in a modern



shell. However, systematic alignment of high/low  $\delta^{18}\text{O}_w$  values with warm/cool seasons implies a real environmental forcing.

We propose that subsurface injection of freshwater from the Central Lens into South Shore coastal waters, driven by changes in sea surface height affecting hydrologic gradients in the subsurface aquifer, cause the  $\sim 0.5\text{‰}$  variations in coastal  $\delta^{18}\text{O}_w$  seen today on tidal timescales along the South Shore. We suggest this mechanism could have also been operating in the past to drive seasonal variations in  $\delta^{18}\text{O}_w$  recorded in fossil shells, with changes in sea surface height driven by seasonal thermal expansion. Altogether, our results highlight the importance of variations in  $\delta^{18}\text{O}_w$  as well as temperature in setting carbonate  $\delta^{18}\text{O}$ . They also suggest that the assumption of constant  $\delta^{18}\text{O}_w$  fails at this site and common assumptions like this may lead to less accurate reconstructions of paleotemperature at other sites.

### Data Availability Statement

Coinciding with publication, all raw clumped isotope data (including all sample and standards replicates) will be deposited in the EarthChem ClumpDB database for long-term storage, data DOI: 10.26022/IEDA/111922 (<https://doi.org/10.26022/IEDA/111922>).

### Acknowledgements

The authors thank Lora Wingate for stable isotope laboratory assistance, Phoebe Aron, Chris Poulsen and the IPL laboratory at the University of Michigan for their discussions, Maria Marcano and Ricardo Anderson for additional modern water sample collection, and Mark Rowe for field assistance. This research was supported by NSF grant 1903237, University of Michigan ADVANCE Crosby Research Award to S. V. Petersen, and NSF GRFP, Rackham Graduate School Merit Fellowship, University of Michigan Turner Grant and Rackham Graduate School Research Grant to J. Z. Zhang.

### References

- Affek, H. P. (2012). Clumped isotope paleothermometry: Principles, applications, and challenges. *Paleontological Society Papers*, 18, 101–114. <https://doi.org/10.1017/s1089332600002576>
- Bajnai, D., Fiebig, J., Tomašových, A., Milner Garcia, S., Rollion-Bard, C., Raddatz, J., et al. (2018). Assessing kinetic fractionation in brachiopod calcite using clumped isotopes. *Scientific Reports*, 8, 1–12. <https://doi.org/10.1038/s41598-017-17353-7>
- Beddows, P. A., Smart, P. L., Whitaker, F. F., & Smith, S. L. (2007). Decoupled fresh-saline groundwater circulation of a coastal carbonate aquifer: Spatial patterns of temperature and specific electrical conductivity. *Journal of Hydrology*, 346(1–2), 18–32. <https://doi.org/10.1016/j.jhydrol.2007.08.013>
- Brocas, W. M., Felis, T., & Mudelsee, M. (2019). Tropical Atlantic cooling and freshening in the middle of the last interglacial from coral proxy records. *Geophysical Research Letters*, 46, 8289–8299. <https://doi.org/10.1029/2019GL083094>
- Buick, D. P., & Ivany, L. C. (2004). 100 years in the dark: Extreme longevity of Eocene bivalves from Antarctica. *Geology*, 32(10), 921–924. <https://doi.org/10.1130/G20796.1>
- Burchell, M., Cannon, A., Hallmann, N., Schwarcz, H. P., & Schöne, B. R. (2013). Refining estimates for the season of shellfish collection on the Pacific Northwest coast: Applying high-resolution stable oxygen isotope analysis and sclerochronology. *Archaeometry*, 55(2), 258–276. <https://doi.org/10.1111/j.1475-4754.2012.00684.x>
- CLIMAP (1984). The Last Interglacial Ocean. *Quaternary Research*, 21, 123–224
- Coates, K. A., Fourqrean, J. W., Kenworthy, W. J., Logan, A., Manuel, S. A., & Smith, S. R. (2013). Introduction to Bermuda: Geology, oceanography and climate. In C. R. C. Sheppard (Ed.), *Coral reefs of the United Kingdom overseas territories* (pp. 115–133). Dordrecht: Springer Netherlands.
- Defliese, W. F., Hren, M. T., & Lohmann, K. C. (2015). Compositional and temperature effects of phosphoric acid fractionation on  $\Delta_{47}$  analysis and implications for discrepant calibrations. *Chemical Geology*, 396(C), 51–60. <https://doi.org/10.1016/j.chemgeo.2014.12.018>
- Defliese, W. F., & Lohmann, K. C. (2016). Evaluation of meteoric calcite cements as a proxy material for mass-47 clumped isotope thermometry. *Geochimica et Cosmochimica Acta*, 173(C), 126–141. <https://doi.org/10.1016/j.gca.2015.10.022>
- Dennis, K. J., Affek, H. P., Passey, B. H., Schrag, D. P., & Eiler, J. M. (2011). Defining an absolute reference frame for 'clumped' isotope studies of CO<sub>2</sub>. *Geochimica et Cosmochimica Acta*, 75(22), 7117–7131. <https://doi.org/10.1016/j.gca.2011.09.025>
- Eagle, R. A., Eiler, J. M., Tripathi, A. K., Ries, J. B., Freitas, P. S., Hiebertal, C., et al. (2013). The influence of temperature and seawater carbonate saturation state on  $^{13}\text{C}$ - $^{18}\text{O}$  bond ordering in bivalve mollusks. *Biogeosciences*, 10(7), 4591–4606. <https://doi.org/10.5194/bg-10-4591-2013>
- Eagle, R. A., Schauble, E. A., Tripathi, A. K., Tütken, T., Hulbert, R. C., & Eiler, J. M. (2010). Body temperatures of modern and extinct vertebrates from  $^{13}\text{C}$ - $^{18}\text{O}$  bond abundances in bioapatite. *Proceedings of the National Academy of Sciences*, 107(23), 10377–10382. <https://doi.org/10.1073/pnas.091115107/-/DCSupplemental>
- Eiler, J. M. (2007). "Clumped-isotope" geochemistry-The study of naturally-occurring, multiply-substituted isotopologues. *Earth and Planetary Science Letters*, 262(3–4), 309–327. <https://doi.org/10.1016/j.epsl.2007.08.020>
- Eiler, J. M. (2011). Paleoclimate reconstruction using carbonate clumped isotope thermometry. *Quaternary Science Reviews*, 30(25–26), 3575–3588. <https://doi.org/10.1016/j.quascirev.2011.09.001>
- Epstein, S., Buchsbaum, R., Lowenstam, H. A., & Urey, H. C. (1953). Revised carbonate-water isotopic temperature scale. *Geological Society of America Bulletin*, 64(11), 1315–1326. [https://doi.org/10.1130/0016-7606\(1953\)64\[1315:RCITS\]2.0.CO;2](https://doi.org/10.1130/0016-7606(1953)64[1315:RCITS]2.0.CO;2)
- Ghosh, P., Adkins, J., Affek, H., Balta, B., Guo, W., Schauble, E. A., et al. (2006).  $^{13}\text{C}$ - $^{18}\text{O}$  bonds in carbonate minerals: A new kind of paleothermometer. *Geochimica et Cosmochimica Acta*, 70(6), 1439–1456. <https://doi.org/10.1016/j.gca.2005.11.014>
- Grossman, E. L., & Ku, T.-L. (1986). Oxygen and carbon isotope fractionation in biogenic aragonite: Temperature effects. *Chemical Geology: Isotope Geoscience section*, 59, 59–74. [https://doi.org/10.1016/0168-9622\(86\)90057-6](https://doi.org/10.1016/0168-9622(86)90057-6)
- Hallmann, N., Schöne, B. R., Strom, A., & Fiebig, J. (2008). An intractable climate archive - Sclerochronological and shell oxygen isotope analyses of the Pacific geoduck, *Panopea abrupta* (bivalve mollusk) from Protection Island (Washington State, USA). *Palaeoecography, Palaeoecology*, 269(1–2), 115–126. <https://doi.org/10.1016/j.palaeco.2008.08.010>
- Harmon, R. S., Mitterer, R. M., Kriausakul, N., Land, L. S., Schwarcz, H. P., Garrett, P., et al. (1983). U-series and amino-acid racemization geochronology of Bermuda: Implications for eustatic sea-level fluctuation over the past 250,000 years. *Palaeoecography, Palaeoecology*, 44, 41–70. [https://doi.org/10.1016/0031-0182\(83\)90004-4](https://doi.org/10.1016/0031-0182(83)90004-4)

- Harrison, S. P., Kutzbach, J. E., Prentice, I. C., Behling, P. J., & Sykes, M. T. (1994). The response of Northern Hemisphere extratropical climate and vegetation to orbitally induced changes in insolation during the last interglaciation. *Quaternary Research*, 43, 174–184.
- Hearty, P. J. (2002). Revision of the late Pleistocene stratigraphy of Bermuda. *Sedimentary Geology*, 153, 1–21. [https://doi.org/10.1016/S0037-0738\(02\)00261-0](https://doi.org/10.1016/S0037-0738(02)00261-0)
- Hearty, P. J., Kindler, P., Cheng, H., & Edwards, R. L. (1999). A +20 m middle Pleistocene Sea-level highstand (Bermuda and the Bahamas) due to partial collapse of Antarctic ice. *Geology*, 27(4), 375–378.
- Hearty, P. J., & Olson, S. L. (2010). Geochronology, biostratigraphy, and changing shell morphology in the land snail subgenus *Poecilozonites* during the Quaternary of Bermuda. *Palaeogeography, Palaeoclimatology, Palaeoecology*, 293(1–2), 9–29. <https://doi.org/10.1016/j.palaeo.2010.04.026>
- Hearty, P. J., Olson, S. L., Kaufman, D. S., Edwards, R. L., & Cheng, H. (2004). Stratigraphy and geochronology of pitfall accumulations in caves and fissures, Bermuda. *Quaternary Science Reviews*, 23(9–10), 1151–1171. <https://doi.org/10.1016/j.quascirev.2003.09.008>
- Hearty, P. J., Vacher, H. L., & Mitterer, R. M. (1992). Aminostratigraphy and ages of Pleistocene limestones of Bermuda. *Geological Society of America Bulletin*, 104(4), 471–480.
- Henkes, G. A., Passey, B. H., Grossman, E. L., Shenton, B. J., Pérez-Huerta, A., & Yancey, T. E. (2014). Temperature limits for preservation of primary calcite clumped isotope paleotemperatures. *Geochimica et Cosmochimica Acta*, 139, 362–382. <https://doi.org/10.1016/j.gca.2014.04.040>
- Henkes, G. A., Passey, B. H., Wanamaker, A. D., Jr, Grossman, E. L., Ambrose, W. G., Jr, & Carroll, M. L. (2013). Carbonate clumped isotope compositions of modern marine mollusk and brachiopod shells. *Geochimica et Cosmochimica Acta*, 106, 307–325. <https://doi.org/10.1016/j.gca.2012.12.020>
- Huntington, K. W., Eiler, J. M., Affek, H. P., Guo, W., Bonifacie, M., Yeung, L. Y., et al. (2009). Methods and limitations of ‘clumped’ CO<sub>2</sub> isotope ( $\Delta_{47}$ ) analysis by gas-source isotope ratio mass spectrometry. *Journal of Mass Spectrometry*, 44(9), 1318–1329. <https://doi.org/10.1002/jms.1614>
- Jacob, J., Ghosh, P., Abdul Jaleel, K. U., Smitha, B. R., Abhilash, K. R., & Sanjeevan, V. N. (2016). Influence of the upwelling events on the  $\delta^{13}\text{C}$  and  $\delta^{18}\text{O}$  of the benthic bivalve shells of the South Western Continental Margin of India. *Environmental Earth Sciences*, 75(2), 1–8. <https://doi.org/10.1007/s12665-015-4954-x>
- Kaspar, F., Kühl, N., Cubasch, U., & Litt, T. (2005). A model-data comparison of European temperatures in the Eemian interglacial. *Geophysical Research Letters*, 32, 2362–2365. <https://doi.org/10.1029/2005GL022456>
- Killingley, J. S., & Berger, W. H. (1979). Stable isotopes in a mollusk shell: Detection of upwelling events. *Science*, 205(4402), 186–188. <https://doi.org/10.1126/science.205.4402.186>
- Kim, S.-T., Mucci, A., & Taylor, B. E. (2007). Phosphoric acid fractionation factors for calcite and aragonite between 25 and 75°C: Revisited. *Chemical Geology*, 246(3–4), 135–146. <https://doi.org/10.1016/j.chemgeo.2007.08.005>
- Kukla, G. J., Bender, M. L., Bond, G., Broecker, W. S., Cleveringa, P., Gavin, J. E., et al. (2002). Last interglacial climates. *Quaternary Research*, 58, 2–13.
- Land, L. S., Mackenzie, F. T., & Gould, S. J. (1967). Pleistocene History of Bermuda. *Geological Society of America Bulletin*, 78, 993–1006. [https://doi.org/10.1130/0016-7606\(1967\)78\[993:phob\]2.0.co;2](https://doi.org/10.1130/0016-7606(1967)78[993:phob]2.0.co;2)
- Meischner, D., Vollbrecht, R., & Wehmeyer, D. (1995). (pp. 1–16). *Pleistocene sea-level yo-yo recorded in stacked beaches, Bermuda South Shore*. Geological Society Special Publications. Retrieved from: <https://doi.org/10.1130/0-8137-2300-0.295>
- Moore, W. S. (1996). Large groundwater inputs to coastal waters revealed by 226Ra enrichments. *Nature*, 380, 612–614. <https://doi.org/10.1038/380612a0>
- Muhs, D. R., Simmons, K. R., & Steinke, B. (2002). Timing and warmth of the Last Interglacial period: New U-series evidence from Hawaii and Bermuda and a new fossil compilation for North America. *Quaternary Science Reviews*, 21, 1355–1383. [https://doi.org/10.1016/S0277-3791\(01\)00114-7](https://doi.org/10.1016/S0277-3791(01)00114-7)
- O’Dea, A., Jackson, J. B. C., Fortunato, H., Smith, J. T., D’Croz, L., Johnson, K. G., & Todd, J. A. (2007). Environmental change preceded Caribbean extinction by 2 million years. *Proceedings of the National Academy of Sciences*, 104, 5501–5506. <https://doi.org/10.1073/pnas.0610947104>
- Olson, S. L., & Hearty, P. J. (2013). Periodicity of extinction and recolonization of the West Indian topshell *Cittarium pica* in the Quaternary of Bermuda (Gastropoda: Trochoidea). *Biological Journal of the Linnean Society*, 110(1), 1–9. [10.1111/bj.12119](https://doi.org/10.1111/bj.12119)
- Petersen, S. V., Defliese, W. F., Saenger, C., Daëron, M., Huntington, K. W., John, C. M., et al. (2019). Effects of Improved <sup>17</sup>O correction on inter-laboratory agreement in clumped isotope calibrations, estimates of mineral-specific offsets, and acid fractionation factor temperature dependence. *Geochemistry, Geophysics, Geosystems*, 20, 3495–3519. [10.1029/2018GC008127](https://doi.org/10.1029/2018GC008127)
- Petersen, S. V., Winkelstern, I. Z., Lohmann, K. C., & Meyer, K. W. (2016). The effects of Porapak trap temperature on  $\delta^{18}\text{O}$ ,  $\delta^{13}\text{C}$ , and  $\Delta_{47}$  values in preparing samples for clumped isotope analysis. *Rapid Communications in Mass Spectrometry*, 30(1), 199–208. <https://doi.org/10.1002/rcm.7438>
- Robertson, R. (2003). The edible West Indian “whelk” *Cittarium pica* (Gastropoda: Trochidae): Natural history with new observations. *Proceedings of the Academy of Natural Sciences of Philadelphia*, 153, 27–47. [https://doi.org/10.1635/0097-3157\(2003\)153\[0027:teiwjc\]2.0.co;2](https://doi.org/10.1635/0097-3157(2003)153[0027:teiwjc]2.0.co;2)
- Rosenheim, B. E., Tang, J., & Fernandez, A. (2013). Measurement of multiply substituted isotopologues (‘clumped isotopes’) of CO<sub>2</sub> using a 5 kV compact isotope ratio mass spectrometer: Performance, reference frame, and carbonate paleothermometry. *Rapid Communications in Mass Spectrometry*, 27, 1847–1857. <https://doi.org/10.1002/rcm.6634>
- Rowe, M. (1984). The freshwater “Central Lens” of Bermuda. *Journal of Hydrology*, 73, 165–176. [https://doi.org/10.1016/0022-1694\(84\)90038-6](https://doi.org/10.1016/0022-1694(84)90038-6)
- Rowe, M. P., Wainer, K. A. I., Bristow, C. S., & Thomas, A. L. (2014). Anomalous MIS 7 sea level recorded on Bermuda. *Quaternary Science Reviews*, 90(C), 47–59. <https://doi.org/10.1016/j.quascirev.2014.02.012>
- Saenger, C., Affek, H. P., Felis, T., Thiagarajan, N., Lough, J. M., & Holcomb, M. (2012). Carbonate clumped isotope variability in shallow water corals: Temperature dependence and growth-related vital effects. *Geochimica et Cosmochimica Acta*, 99, 224–242. <https://doi.org/10.1016/j.gca.2012.09.035>
- Sanchez Goni, M. F., Bakker, P., Desprat, S., Carlson, A. E., Van Meerbeek, C. J., Peyron, O., et al. (2012). European climate optimum and enhanced Greenland melt during the Last Interglacial. *Geology*, 40(7), 627–630. <https://doi.org/10.1130/G32908.1>
- Schmidt, M. W., Spero, H. J., & Lea, D. W. (2004). Links between salinity variation in the Caribbean and North Atlantic thermohaline circulation. *Nature*, 428, 160–163. <https://doi.org/10.1038/nature02346>

- Schöne, B. R., Freyre Castro, A. D., Fiebig, J., Houk, S. D., Oschmann, W., & Kröncke, I. (2004). Sea surface water temperatures over the period 1884–1983 reconstructed from oxygen isotope ratios of a bivalve mollusk shell (*Arctica islandica*, southern North Sea). *Paleogeography, Paleoclimatology, Palaeoecology*, *212*(3–4), 215–232. <https://doi.org/10.1016/j.palaeo.2004.05.024>
- Stolper, D. A., & Eiler, J. M. (2015). The kinetics of solid-state isotope-exchange reactions for clumped isotopes: A study of inorganic calcites and apatites from natural and experimental samples. *American Journal of Science*, *315*(5), 363–411. <https://doi.org/10.2475/05.2015.01>
- Tao, K., Robbins, J. A., Grossman, E. L., & O'Dea, A. (2013). Quantifying upwelling and freshening in nearshore tropical American environments using stable isotopes in modern gastropods. *BMS*, *89*(4), 815–835. <https://doi.org/10.5343/bms.2012.1065>
- Thiagarajan, N., Adkins, J., & Eiler, J. (2011). Carbonate clumped isotope thermometry of deep-sea corals and implications for vital effects. *Geochimica et Cosmochimica Acta*, *75*(16), 4416–4425. <https://doi.org/10.1016/j.gca.2011.05.004>
- Tripathi, A. K., Eagle, R. A., Thiagarajan, N., Gagnon, A. C., Bauch, H., Halloran, P. R., & Eiler, J. M. (2010).  $^{13}\text{C}$ - $^{18}\text{O}$  isotope signatures and 'clumped isotope' thermometry in foraminifera and coccoliths. *Geochimica et Cosmochimica Acta*, *74*(20), 5697–5717. <https://doi.org/10.1016/j.gca.2010.07.006>
- Tripathi, A., Zachos, J., Marinovich, L., Jr, & Bice, K. (2001). Late Paleocene Arctic coastal climate inferred from molluscan stable and radiogenic isotope ratios. *Paleogeography, Paleoclimatology, Palaeoecology*, *170*, 101–113. [https://doi.org/10.1016/s0031-0182\(01\)00230-9](https://doi.org/10.1016/s0031-0182(01)00230-9)
- Turney, C. S. M., & Jones, R. T. (2010). Does the Agulhas Current amplify global temperatures during super-interglacials? *Journal of Quaternary Science*, *25*(6), 839–843. <https://doi.org/10.1002/jqs.1423>
- Vacher, H. L. (1978). Hydrogeology of Bermuda - Significance of an across-the-island variation in permeability. *Journal of Hydrology*, *39*, 207–226. [https://doi.org/10.1016/0022-1694\(78\)90001-x](https://doi.org/10.1016/0022-1694(78)90001-x)
- Vacher, H. L., & Rowe, M. P. (1997). Geology and Hydrogeology of Bermuda. *Developments in Sedimentology*, *54*, 35–90.
- Vacher, H. L., & Wallis, T. N. (1992). Comparative hydrogeology of fresh-water lenses of Bermuda and Great Exuma Island, Bahamas. *Ground Water*, *30*, 15–20. <https://doi.org/10.1111/j.1745-6584.1992.tb00806.x>
- van Hengstum, P. J., & Scott, D. B. (2012). Sea-level rise and coastal circulation controlled Holocene groundwater development in Bermuda and caused a meteoric lens to collapse 1600years ago. *Marine Micropaleontology*, *90–91*, 29–43. <https://doi.org/10.1016/j.marmicro.2012.02.007>
- Vollbrecht, R. (1990). Marine and meteoric diagenesis of submarine pleistocene carbonates from the Bermuda carbonate platform. *Carbonates and Evaporites*, *5*, 1–84. <https://doi.org/10.1007/bf03174319>
- Walker, S. E. (1994). Biological Remanie: Gastropod fossils used by the living terrestrial hermit crab, *coenobita clypeatus*, on Bermuda. *Palaios*, *9*, 403–412. <https://doi.org/10.2307/3515058>
- Wanamaker, A. D., Jr, Kreutz, K. J., Borns, H. W., Jr, Introne, D. S., Feindel, S., & Barber, B. J. (2006). An aquaculture-based method for calibrated bivalve isotope paleothermometry. *Geochemistry, Geophysics, Geosystems*, *7*, Q09011. <https://doi.org/10.1029/2005GC001189>
- Wanamaker, A. D., Jr, Kreutz, K. J., Schöne, B. R., Pettigrew, N., Borns, H. W., Introne, D. S., et al. (2008). Coupled North Atlantic slope water forcing on Gulf of Maine temperatures over the past millennium. *Climate Dynamics*, *31*(2–3), 183–194. <https://doi.org/10.1007/s00382-007-0344-8>
- Whitaker, F. F., & Smart, P. L. (1990). Active circulation of saline ground waters in carbonate platforms: Evidence from the Great Bahama Bank. *Geology*, *18*, 200–203. [https://doi.org/10.1130/0091-7613\(1990\)018<0200:acosgw>2.3.co;2](https://doi.org/10.1130/0091-7613(1990)018<0200:acosgw>2.3.co;2)
- Winkelstern, I. Z., Rowe, M. P., Lohmann, K. C., Defliese, W. F., Petersen, S. V., & Brewer, A. W. (2017). Meltwater pulse recorded in Last Interglacial mollusk shells from Bermuda. *Paleoceanography*, *32*(2), 132–145. <https://doi.org/10.1002/2016PA003014>
- Winkelstern, I. Z., Surge, D., & Hudley, J. (2013). Multiproxy sclerochronological evidence for Plio-Pleistocene regional warmth: United States mid-Atlantic coastal plain. *Palaios*, *28*, 649–660.